energies

MDPI

Article

Distributed Resilient Voltage and Reactive Power Control for Islanded Microgrids under False Data Injection Attacks

Liang Ma * and Gang Xu

School of Electrical and Electronic Engineering, North China Electric Power University, Beijing 102206, China; xugang@ncepu.edu.cn

* Correspondence: nick_m276@163.com; Tel.: +86-186-1222-7468

Received: 16 June 2020; Accepted: 23 July 2020; Published: 25 July 2020

Abstract: This paper addresses the problem of voltage and reactive power control of inverter-based distributed generations (DGs) in an islanded microgrid subject to False Data Injection (FDI) attacks. To implement average voltage restoration and reactive power sharing, a two-layer distributed secondary control framework employing a multiagent system (MAS)-based dynamic consensus protocol is proposed. While communication network facilitates distributed control scheme, it leads to vulnerability of microgrids to malicious cyber-attacks. The adverse effects of FDI attack on the secondary controller are analyzed, and the necessary and sufficient conditions to model stealthy attack and probing attack are discussed in detail. A trust-based resilient control strategy is developed to resist the impacts of FDI attack. Based on the forward-backward consistency criterion, the self-monitoring and neighbor-monitoring mechanisms are developed to detect the misbehaving DGs. A group decision-making mechanism is also introduced to settle conflicts arising from the dishonest trust index caused by colluding attacks. A novel mitigation countermeasure is designed to eliminate the adversarial effects of attack: the discarding information mechanism is used to prevent the propagation of false data in the cooperative network while the recovery actions are designed to correct the deviations of collective estimation error in both transient disturbance and continuous FDI attack scenarios. Through a theoretical analysis, it is proved that the proposed mitigation and recovery mechanism can maintain the correct average estimates of voltage and reactive power, which ensures the secondary control objectives of microgrids under FDI attack. Simulation results on an islanded microgrid show the effectiveness and resilience of the proposed control scheme.

Keywords: microgrids; voltage restoration; reactive power sharing; false data injection attacks; trust; resilience

1. Introduction

Due to the rapid advances and wide applications of measurements, communication and computation technology, the traditional power grid has been experiencing a revolution towards a smart grid, which can enhance reliability, safety and efficiency of power system [1]. In order to overcome the intermittent characteristics of distributed generations (DGs), as well as fully exploit the benefit of DGs, microgrids are gradually playing an important role in the smart grids [2]. A microgrid is able to operate in grid-connected or islanded mode, and transfer between these two modes seamlessly. In an islanded microgrid, the traditional droop-based primary control introduces voltage and frequency deviations from their nominal values. Due to the mismatch of line impedance, primary control is unable to achieve reactive power sharing among DGs, which impairs the dynamic performance and power supply quality of microgrids [3,4].

Various hierarchical control frameworks consisting of primary, secondary and tertiary control levels have been proposed to improve the performance of microgrids [5]. To stabilize the voltage and frequency of microgrids, the primary control is designed mainly based on the droop technique, which relies on only local information of each DG unit [6]. The secondary control is necessary to compensate for the steady-state error of the voltage and frequency caused by primary droop control and to restore the voltage and frequency to their nominal values. The tertiary control is aimed at optimizing the operating cost and energy management of microgrids. In general, centralized control and distributed control are two common strategies in secondary control level [7]. In traditional centralized strategy, a central control unit and a complicated fully-connected communication network are required to collect information from all DGs. Under such circumstance, any single point of failure may cause instability of the entire system, which impairs the reliability of microgrids. The multiagent system (MAS) -based distributed control strategy has been proposed as a promising solution to electric grids with increasing penetration of DGs [8–10]. In contrast to the centralized scheme, the MAS-based distributed control scheme has the following advantages: (1) Centralized scheme requires a high bandwidth network to collect system-wide information, while MAS-based scheme only relies on local information exchange among neighboring DGs. As a result, the sparse communication network can be used for MAS-based distributed scheme, which significantly reduces the communication cost. (2) Without any reliance on a centralized control unit, the MAS-based distributed scheme is more suitable to handle topology variations and plug-and-play operations, which enhances the scalability and flexibility of microgrids. (3) MAS-based distributed control scheme ensures more robust performance under imperfect communication situations, such as time delay and noise [11]. Thus, the reliability of system can be improved compared to the centralized scheme.

Despite their remarkable advantages, distributed control schemes are more vulnerable to malicious cyber-attacks since they lack the capacity of global situation awareness. Cyber-attacks are considered as serious threats to the security of networked control systems and have received great concern in both industrial and academic fields. Roughly, cyber-attacks can be categorized into: Denial-of-Service (DoS) attacks and False Data Injection (FDI) attacks. The DoS attack aims to make information unavailable by blocking legitimate data transmissions, while the FDI attack aims to modify the integrity of transmitted data packets [12]. To design a resilient control strategy, it is of significance to identify the adverse effects of FDI attack on the system performance from the attackers' perspective [13]. If the attackers have obtained the prior knowledge about the communication topology and control protocol of the microgrid system, such intelligent attackers can inject coordinated attack signals in multiple nodes without exposing themselves to any intrusion detection system [14,15]. With regards to distributed control theory, asymptotic convergence of agents can still be achieved under such type of attack, even though the final operating state may be incorrect. In this case, the control objectives of microgrids will be maneuvered artificially by the attackers. Thus, the study of the impacts of FDI attack on distributed microgrids controller is of both theoretical merit and practical value.

Much research work has been conducted in cyber-attacks on the power grid with centralized control structure [16]. Security and resilience is an area of growing concern for the smart power grid applications, such as power system state estimation, electricity market and Phasor Measurement Unit (PMU) data [17]. Conventional resilient control strategies such as observer-based state reconstruction [18], state prediction-aided method [19] and machine learning-based attack detection mechanism [20] have been proposed to mitigate the vulnerability caused by malicious cyber-attacks. However, these strategies assume a control center to collect system-wide information, which is not suitable for the distributed control structure of microgrids. Although the machine learning-based intrusion detection mechanism is model independent, it requires a huge historical data set for training the algorithms. The lack of the corresponding data set containing multiple attack scenarios hinder the further application on this method in microgrids.

With regard to distributed secondary control scheme of microgrids under cyber-attacks, only few efforts have been reported in the aspect of intrusion detection mechanisms and mitigation measures.

A transient model -based technique was proposed to detect FDI attacks on the centralized controller of microgrids in [21]. In [22], a stable region concept was proposed, in which the impacts of FDI attack on the utilization level of microgrids were discussed, but no mitigation countermeasures were presented. In [23], a FDI attack was detected by the variation of the candidate invariants. However, this approach requires accurate model checking tools, which increases the computational burden and complications. A signal temporal logic (STL)-based attack detection mechanism was proposed in [24]. The upper and lower bounds of the voltage and current were estimated, and the state information falling out of the bounds implies the presence of attack. However, it should be noted that false states, even within the given bounds, could cause large deviations in the final operation point. In [25], a leader-follower consensus algorithm was used to restore the frequency of an islanded microgrid. The proposed distributed observer strategy can only reconstruct the constant attack signals, and the assumption of an attack-free leader should be guaranteed. The extended state observer (ESO) method was presented in [26] to estimate the disturbance signals including FDI attack on microgrids. However, the derivative of disturbance signals should be zero in the steady state, and the situation that ESO itself may be attacked by adversaries is not considered. The trust-based resilient control approaches were introduced to the distributed energy management [27], cognitive radio sensor network [28], and unmanned aerial vehicles system [29] to minimize the adverse effects of malicious attacks. However, these approaches fail to consider the colluding attacks, which can manipulate the trust value of agents and lead to the failure of the proposed defense mechanism. To the author's knowledge, little research has been conducted to take into account the effects of FDI attack on voltage and reactive power coordination of an islanded microgrid, and the resilient secondary control scheme design has not been discussed, which motivates the current study.

In this paper, we focus on the attack detection and mitigation techniques to improve the resilience of distributed voltage and reactive power control of islanded microgrids with respect to FDI attack. Unlike the grid-connected microgrids in which voltage and frequency are supported by the main grid, the control scheme to coordinate multiple DGs directly affects the voltage and frequency stability, power sharing and dynamic performance of islanded microgrids. Furthermore, the low rating of DGs, lack of static compensation devices, and line impedance mismatch requires an accurate reactive power sharing to avoid overloading to cause damage of DGs [9,10]. A two-layer distributed control scheme is presented to implement average voltage restoration and reactive power sharing, in which a MAS-based dynamic consensus protocol is employed to estimate the average voltage and reactive power, and a PI controller is designed to compensate for the deviations caused by the primary control. A trust-based control scheme is proposed to resist the impacts of FDI attack on the microgrid control system. The main contribution of this paper is summarized as follows: (1) The adverse effects of FDI attack on the proposed voltage and reactive power control scheme are analyzed in detail. The necessary and sufficient conditions for attackers to conduct stealthy attack and probing attack are discussed according to the cumulative effect of the injected false data. (2) A trust-based resilient control strategy is proposed, in which the trust evaluation result manipulated by the colluding attack is considered. A forward-backward consistency criterion is designed to detect the misbehaving DGs, and a group decision-making mechanism is introduced to settle conflicts arising from the dishonest trust index caused by colluding attack. (3) A novel mitigation countermeasure is proposed to eliminate the impacts of FDI attack. An information discarding mechanism is designed to prevent the propagation of false data in the cooperative network. Through a theoretical analysis, we show that the proposed recovery actions can correct the deviations of the collective estimation error caused by the attack, in both transient disturbance and continuous FDI attack scenarios. Consequently, the correct average estimates of voltage and reactive power can be maintained and the secondary control objectives are not affected by FDI attack.

The rest of this paper is organized as follows: Section 2 depicts the cyber physical architecture of the islanded microgrid along with the distributed secondary control to achieve average voltage restoration and reactive power sharing. Section 3 presents the adverse effects of FDI attack on the

proposed distributed control scheme, and the conditions for attackers to conduct stealthy attack and probing attack are given in detail. Section 4 provides the trust-based resilient control framework to detect attack and eliminate the impacts of false data on the secondary control objectives. Simulation results and discussion are presented in Section 5. Finally, the conclusions are drawn in Section 6.

2. Secondary Voltage and Reactive Power Control for Islanded Microgrids

2.1. Cyber-Physical Model of Islanded Microgrids

Figure 1 presents the cyber-physical model of an islanded AC microgrid containing several DGs. In the physical layer of the microgrid, three-phase inverter-based DG_i ($i = 1, \ldots, N$) is connected to the microgrid through a DC/AC inverter, an LC filter and a output connector. L_i^s, R_i^s and C_i^s represent the inductance, resistance and capacitance of the LC filter, while L_i^c and R_i^c represent the inductance and resistance of the output connector.

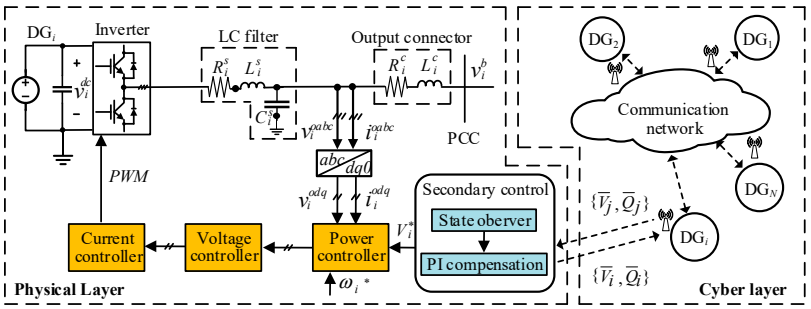

Figure 1. Cyber-physical model of an islanded microgrid.

As shown in Figure 1, the primary control of DG_i includes the droop-based power controller, PI voltage controller and PI current controller. For DG_i, the droop technique used in power controller mimics the droop mechanism of the traditional synchronous generator to regulate angular frequency ω_i and voltage V_i according to active and reactive power respectively, and can be given by [8,10]:

$$\begin{cases} V_i = V_i^* - n_i^Q Q_i \\ \omega_i = \omega_i^* - m_i^p P_i \end{cases} \quad (1)$$

where m_i^p and n_i^Q are the frequency and voltage droop coefficients. P_i and Q_i are the fundamental components of active and reactive power, which can be obtained via two low-pass filters. ω_i^* and V_i^* are the reference signals for primary control, and V_i^* is derived by the secondary control in this paper.

In the cyber layer, each DG is considered as an agent which shares information with its neighbors through a sparse communication network. The communication network is described as an undirected graph $G = (V, \Xi)$, where $V = \{1, \ldots, N\}$ denotes the set of nodes corresponding to DGs, and $\Xi \subset V \times V$ is the set of edges corresponding to the communication links. Node j is a neighbor of node i if there exists an edge defined as $(i,\ j) \in \Xi$. $W = \left[w_{ij}\right] \in R^{N \times N}$ is defined as the adjacency matrix, where $w_{ii} = 0$ for all i, and $w_{ij} = 1$ if $(i,\ j) \in \Xi$, otherwise, $w_{ij} = 0$. $N_i = \{j \left| (i,\ j) \in \Xi \right.\}$ represents the set of neighbors of node i, and the degree of node i is defined as $d_i = \sum_{j \epsilon N_i} w_{ij}$. The Laplacian matrix L of the graph G is expressed as $L = D - W$, where $D = \mathrm{diag}\{d_1, d_2, \ldots, d_N\}$ is the degree matrix of the graph. A path is defined as a connected edge in a graph, and the graph G is connected if there is a path between any two nodes.

2.2. Distributed Secondary Control Framework for Voltage and Reactive Power

The droop characteristic of primary control makes the voltages of DGs deviate from the rated value. Meanwhile, accurate reactive power sharing among DGs cannot be achieved due to the line

impedance mismatch. The objective of the secondary control in this paper is to restore the average voltage to the rated value while maintaining reactive power sharing of among DGs. Figure 2 shows the proposed framework for voltage and reactive power control, which involves estimation sublayer and compensation sublayer. The estimation sublayer is responsible to obtain the average information of voltage and reactive power in a distributed manner, then sends it to the compensation sublayer. The compensation sublayer calculates the reference signal V_i^* and sends it to the primary control to regulate average voltage and achieve reactive power sharing among DGs.

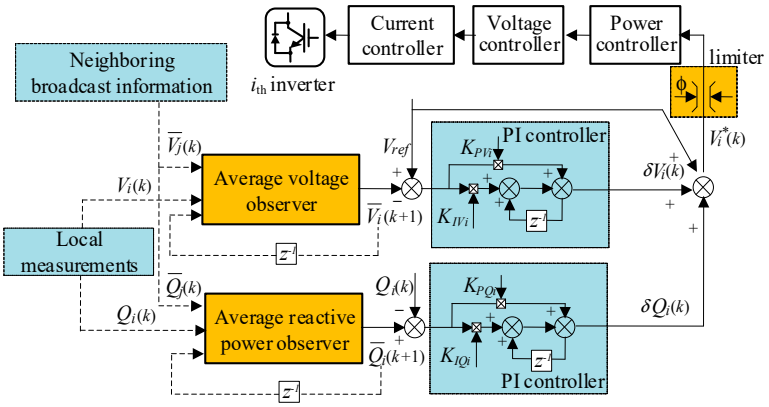

Figure 2. Proposed cooperative control for average voltage restoration and reactive power sharing.

(1) Estimation sublayer: For global average voltage restoration and reactive power sharing, a state observer based on discrete dynamic consensus algorithm [30] is proposed to acquire the average information of voltage and reactive power. At each iteration k, $\overline{x}_i(k) = \left\{\overline{V}_i(k),\ \overline{Q}_i(k)\right\}$ $(i = 1, \ldots, N)$ denotes the average estimates of voltage and reactive power. DG_i receives the neighboring estimates $\overline{x}_j(k) = \left\{\overline{V}_j(k),\ \overline{Q}_j(k)\right\}$ $\forall j \in N_i$ via the communication network, and the state observer is updated as:

$$\begin{cases} \overline{V}_i(k+1) = \overline{V}_i(k) + \underbrace{\varepsilon \sum_{j \in N_i} w_{ij}\left(\overline{V}_j(k) - \overline{V}_i(k)\right)}_{u_{i,V}(k)} + V_i(k+1) - V_i(k) \\ \overline{Q}_i(k+1) = \overline{Q}_i(k) + \underbrace{\varepsilon \sum_{j \in N_i} w_{ij}\left(\overline{Q}_j(k) - \overline{Q}_i(k)\right)}_{u_{i,Q}(k)} + Q_i(k+1) - Q_i(k) \end{cases} \tag{2}$$

where $x_i(k) = \{V_i(k),\ Q_i(k)\}$ denotes the measured voltage and reactive power of DG_i. ε is the step-size which should satisfy $0 < \varepsilon < (1/max_{i=1,\ldots,N} d_i)$ to ensure the convergence of algorithm. $u_i(k) = \left\{u_{i,V}(k),\ u_{i,Q}(k)\right\}$ denotes the cooperative control input.

By referring to Theorem 3.1 in [30], summing $\overline{x}_i(k)$ in Equation (2) over all agents, then the following equation can be obtained:

$$\sum_{i \in V} \overline{x}_i(k+1) = \sum_{i \in V} \overline{x}_i(k) + \varepsilon \sum_{i \in V} \sum_{j \in N_i} w_{ij}\left(\overline{x}_j(k) - \overline{x}_i(k)\right) + \sum_{i \in V} (x_i(k+1) - x_i(k)) \tag{3}$$

In Equation (3), the summation $\sum_{i\in \mathrm{V}} \sum_{j\in N_i} \left(\overline{x}_j(k) - \overline{x}_i(k)\right)$ always equals to zero, because the communication topology is an undirected graph and for all i and j we have $w_{ij} = w_{ji}$, every term in the summation has its opposite counterpart. The initialization condition of Equation (2) is set as $\overline{x}_i(0) = x_i(0)$, then $\sum_{i\in \mathrm{V}} \overline{x}_i(k) = \sum_{i\in \mathrm{V}} x_i(k)$ always holds true during the iteration process. Under the effects of the cooperative control input, we have $\lim_{k\to\infty} \overline{x}_i(k) = \lim_{k\to\infty} x_i(k)$. Therefore, $\overline{x}_i(k)$ converges to the average value of voltage and reactive power, which can be expressed as:

$$\begin{cases} \lim_{k\to\infty} \overline{V}_i(k) = \frac{1}{N} \lim_{k\to\infty} \sum_{i\in \mathrm{V}} V_i(k) \\ \lim_{k\to\infty} \overline{Q}_i(k) = \frac{1}{N} \lim_{k\to\infty} \sum_{i\in \mathrm{V}} Q_i(k) \end{cases} \tag{4}$$

Remark 1. *The traditional control for the voltage restoration and reactive power sharing of an islanded microgrid employs a centralized structure [31], in which the measurement information of overall DGs is required to calculate the average value. Different from the traditional centralized way, the state observer with dynamic consensus algorithm enables DGs to estimate the average voltage and reactive power in a fully distributed manner. Furthermore, considering the discrete nature of communication data transmission in the secondary control level of the microgrid, the discrete time-based method is more suitable for the engineering practice.*

(2) Compensation sublayer: To achieve average voltage regulation, each DG requires to measure the voltage error and compensates for the deviation caused by the primary control. Meanwhile, the average reactive power estimate serves as the reference value for each DG to realize reactive power sharing. Two compensation terms for DG_i are calculated using [31]:

$$\begin{cases} \delta V_i(k) = K_{PVi}^{AVE}\left(V_{ref} - \overline{V}_i(k)\right) + K_{IVi}^{AVE} \sum_{p=0}^{k} \left(V_{ref} - \overline{V}_i(p)\right) \\ \delta Q_i(k) = K_{PQi}^{AVE}\left(\overline{Q}_i(k) - Q_i(k)\right) + K_{IQi}^{AVE} \sum_{p=0}^{k} \left(\overline{Q}_i(p) - Q_i(p)\right) \end{cases} \tag{5}$$

where K_{PVi}^{AVE} and K_{IVi}^{AVE} are the proportional and integral gains of PI controller for average voltage restoration, and K_{PQi}^{AVE} and K_{IQi}^{AVE} are the proportional and integral gains of PI controller for reactive power sharing. V_{ref} denotes the global reference voltage for all DGs. The compensation terms obtained in (5) are finally added to V_{ref}, and the reference signal V_i^* sent to the primary control of DG_i can be calculated as:

$$V_i^*(k) = V_{ref} + \delta V_i(k) + \delta Q_i(k) \tag{6}$$

The secondary controller typically includes the voltage limiter (see Figure 2). This limiter is responsible to carry out two tasks: it limits the voltage variations at terminal of each DG and limits the transmission line loading. According to Figure 2, the output voltage of each DG is limited to $V_{ref} - \phi \le V_i^* \le V_{ref} + \phi$ to prevent voltage from exceeding the boundary.

With adoption of the cooperative dynamic consensus algorithm and the PI controllers for a connected communication topology for a microgrid, the solutions in Equation (2) shall converge to:

$$\lim_{k\to\infty} \overline{V}_i(k) = V_{ref},\ \lim_{k\to\infty} \overline{Q}_i(k) = \frac{1}{N} \lim_{k\to\infty} \sum\nolimits_{i\in V} Q_i(k),\ \forall i \in V \tag{7}$$

The above equation indicates that the control objectives of average voltage restoration and reactive power sharing can be achieved by the proposed control framework. However, for injecting false data into a single or multiple agents, abnormal discontinuity will be introduced in updating Equation (2), which disrupts the consensus between agents and ultimately affects the final convergence results in

Equation (7). The modeling of such attack and its impacts on the proposed secondary voltage and reactive power control scheme is discussed in the following section.

3. Vulnerability Analysis of the Distributed Control Scheme Subject to FDI Attack

Considering that the attackers penetrate into the control system of the microgrid and inject false data into the proposed distributed cooperative controller, the adverse effects of FDI attack on the convergence is discussed in detail in this section.

In the MAS-based cooperative control framework, each DG is considered as an agent. When the attacker conduct FDI attack to some agents, these agents will become misbehaving agents [15,25,27]. The misbehaving agents will be manipulated to inject false data into the state variables $\overline{V}_i(k)$ and $\overline{Q}_i(k)$ in Equation (2), where DG_i is an misbehaving agent and k denotes the step of the iterative process. Thus, we propose a general form of the algorithm (2) under FDI attack which can be modeled as:

$$\begin{cases} \overline{V}_i(k+1) = \overline{V}_i(k) + u_{i,V}(k) + V_i(k+1) - V_i(k) + f^a_{i,V}(k) \\ \overline{Q}_i(k+1) = \overline{Q}_i(k) + u_{i,Q}(k) + Q_i(k+1) - Q_i(k) + f^a_{i,Q}(k) \end{cases} \tag{8}$$

where DG_i is the misbehaving DG, $f^a_{i,V}(k)$ and $f^a_{i,Q}(k)$ represent the false data injected into $\overline{V}_i(k)$ and $\overline{Q}_i(k)$, respectively.

It can be observed from Equation (8) that the attacker can easily ruin the convergence of the proposed cooperative controller (2). However, if the attacker breaks the convergence, the system operator or the agents can easily know the presence of attack. From the attackers' perspective, the attack activities should keep stealthy to make them less detectable by the intrusion detection mechanism of the microgrid system. To design a resilient control scheme, it is crucial to understand the adverse effects of such undetectable attacks.

Define $\overline{x}(k) = [\overline{x}_1(k), \overline{x}_2(k), \ldots, \overline{x}_N(k)]^T$ as the vector of voltage and reactive power estimates, $f^a_V(k) = \left[f^a_{1,V}(k), f^a_{2,V}(k), \ldots, f^a_{N,V}(k)\right]^T$ and $f^a_Q(k) = \left[f^a_{1,Q}(k), f^a_{2,Q}(k), \ldots, f^a_{N,Q}(k)\right]^T$ represent the vectors of false data injected to the cooperative controllers. The solution of Equation (8) under the attack can be expressed as [32]:

$$\overline{x}(k) = A_c^k \overline{x}(0) + \sum_{p=0}^{k-1} A_c^{k-p-1}(x_i(p+1) - x_i(p)) + \sum_{p=0}^{k-1} A_c^{k-p-1} f^a(p) \tag{9}$$

where $A_c = I - \varepsilon L$ is the closed-loop matrix. $f^a(k) = \left\{f^a_V(k), f^a_Q(k)\right\}$ denotes the overall attack signals at k iteration. By referring to [30], the global dynamic of Equation (9) in steady state can be given by:

$$\overline{x}(k) \to \frac{\mathbf{1}_N}{N} \sum_{i=1}^{N} x_i(k) + \sum_{p=0}^{k-1} A_c^{k-p-1} f^a(p) \tag{10}$$

where $\mathbf{1}_N = [1, 1, \ldots, 1]^T$. In Equation (10), the first term on the right-hide side represents the desired consensus value (i.e., the average value of voltage and reactive power), and the second term reflects the cumulative effect of the attack signals on the cooperative controller. It can be seen that the attacker can disrupt the convergence of the algorithm by injecting false data to the control system. However, in order to keep the attacks undetectable to the system operator or the intrusion detection mechanism, smart attackers can adjust the cumulative effect of attack signals to manipulate the final operating state of microgrids while maintaining the convergence of Equation (10).

Definition 1. *Stealthy attack. The cumulative effect of attack signals on cooperative control is limited for the iteration process. If there exists a constant H such that:*

$$\sum_{k=0}^{\infty}|f_{i,V}^{a}(k)| \le H,\ \sum_{k=0}^{\infty}|f_{i,Q}^{a}(k)| \le H,\ \forall i \in \mathrm{V} \tag{11}$$

Then, the attack makes Equation (10) converges to an incorrect stable point, that

$$\lim_{k\to\infty}\overline{V}_i(k) = V_{ref}^{a},\ \lim_{k\to\infty}\overline{Q}_i(k) = Q^{a},\ \forall i \in \mathrm{V} \tag{12}$$

where $V_{ref}^{a} \neq V_{ref}$ *and* $Q^{a} \neq \frac{1}{N}\sum_{i\in V} Q_i(k)$.

According to Equation (10), A_c has a simple eigenvalue 1 and all other eigenvalues lie in the open unit disk. By referring to [32], $\lim_{k\to\infty}\sum_{p=0}^{\infty} A_c^{k-p-1} f^{a}(p)$ will converge to a nonzero constant, i.e., $\lim_{k\to\infty}\sum_{p=0}^{\infty} A_c^{k-p-1} f^{a}(p) = c$, where c is a constant. Thus, it can be obtained that the final value of Equation (10) will converge to $\lim_{k\to\infty}\overline{x}_i(k) = \frac{1}{N}\lim_{k\to\infty}\sum_{i\in V} x_i(k) + c$. In this case, we can observe that $\overline{V}_i(k)$ and $\overline{Q}_i(k)$ converge to a stable but incorrect final point, which will affect the control objectives of the proposed secondary control scheme.

Remark 2. *The condition Equation (11) shows that, the attacker without any prior knowledge of system can still manipulate the final operating state of microgrids while maintaining the convergence of the cooperative control. When the convergence is achieved, each agent will think that the average estimates of voltage and reactive power are acquired, thus such kind of attack is stealthy.*

Definition 2. *Probing attack. The cumulative effect of attack signals on cooperative control is zero for the iteration process. If the attack signals satisfy condition Equation (11) and the following equation holds,*

$$\lim_{k\to\infty}\sum_{k=0}^{\infty}\sum_{i\in V} f_{i,V}^{a}(k) = 0,\ \lim_{k\to\infty}\sum_{k=0}^{\infty}\sum_{i\in V} f_{i,Q}^{a}(k) = 0,\ \forall i \in \mathrm{V} \tag{13}$$

the control objectives in Equation (7) can still be achieved in steady state even under probing attack.

By summing $\overline{x}(k+1)$ in Equation (8) over all DGs, the following equation holds:

$$\begin{aligned}\sum_{i\in V}\overline{x}_i(k+1) &= \sum_{i\in V}\overline{x}_i(k) + \sum_{i\in V}(x_i(k+1) - x_i(k)) + \sum_{i\in V} f_i^{a}(k)\\ &= \sum_{i\in V}\overline{x}_i(0) + \sum_{i\in V}(x_i(k+1) - x_i(0)) + \sum_{p=0}^{k}\sum_{i\in V} f_i^{a}(p)\end{aligned} \tag{14}$$

Since the initialization condition is set as $\overline{x}_i(0) = x_i(0)$, if the condition $\sum_{p=0}^{k}\sum_{i\in V} f_i^{a}(p) = 0$ is satisfied, $\sum_{i\in V}\overline{x}_i(k+1) = \sum_{i\in V} x_i(k+1)$ will hold. Thus, the correct average estimates of voltage and reactive power can still be acquired and the steady state of the microgrid will not be affected.

Remark 3. *The condition Equation (13) indicates that the attacker can intrude the control system of the microgrid without causing any adverse effects on the objectives of the secondary control. By injecting zero-sum attack signals into a single agent or symmetric attack signals into multiple agents, probing attack can help the attacker to confirm the success of intrusion and prepare for more serious attacks in the long run process.*

Definition 3. *Destabilization attack. If the attack signals cannot satisfy the conditions Equations (11) and (13), the final convergence of the agents will be ruined, leading to the failure of the cooperative control.*

Remark 4. *According to Equation (10),* $l_{ij}^m = [I - \varepsilon L]_{ij}^m$ *with* $[\,]_{ij}$ *denotes the element* (i, j) *of a matrix, and* m *represents the length of the shortest path from agent* j *to agent* i*. It can be easily seen that an attack on a compromised agent can affect the intact agents that are reachable from it. That is, an attack on a single agent can propagate in the cooperative network, which even destabilizes the entire system. However, from the attackers' perspective, the duration of FDI attack should be as short as possible to make them less detectable. Thus, the FDI attack should not span the entire time to avoid the attacker exposed to the detection mechanism.*

To show the adverse effects of the abovementioned attack strategies on the proposed cooperative controller (2), a case study is presented in Figure 3. The microgrid test system consists of five DGs and three loads. The detailed control parameters and communication topology are presented in Section 5. As illustrated in Figure 3, the microgrid works in islanded mode from $t = 0$ s, and the proposed secondary controller is applied at $t = 0.5$ s. Then the average voltage of DGs can gradually restore to the rated value 380 V while maintaining the accurate reactive power sharing. From 1.5 s to 2 s, the probing attack signals 0.3 V and −0.3 V are injected into DG_1 and DG_4 according to Equation (8), such that the cumulative effect of FDI attack meets the condition Equation (13). After the attack is removed at $t = 2$ s, it can be seen that $\overline{V}(k)$ and $\overline{Q}(k)$ gradually converge to their respective normal values as stated in Equation (7). The control objectives can still be achieved under such type of attack. From 3 s to 3.3 s, a stealthy attack signal $f_{4,Q}^a(k) = 300 - 10 \times (k - 300)$ kVar is injected into the average reactive power controller of DG_2. We observe that the convergence of the control scheme are not ruined, but the final stable points of $\overline{V}(k)$ and $\overline{Q}(k)$ are affected by the attack, which leads to abnormal increase of voltage and reactive power of each DG. At $t = 4.5$ s, the destabilization attack is initiated with a sinusoidal attack signal injected into the average reactive power controller of DG_5. One can observe that the compromised DG_5 can affect the other intact DGs and the false data propagates in the cooperative network which causes instability of the entire system.

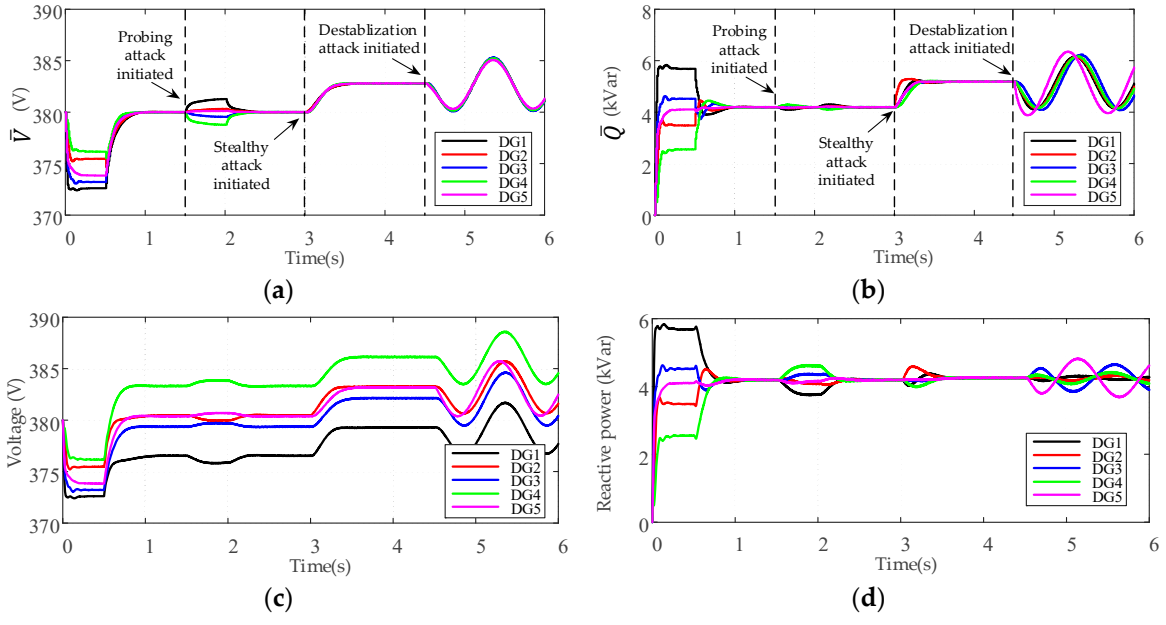

Figure 3. The different adverse effects of FDI attack on the proposed cooperative controller: (**a**) Average voltage estimate; (**b**) Average reactive power estimate; (**c**) Voltages of DGs; (**d**) Reactive power of DGs.

4. Trust-Based Resilient Control Framework for Microgrids against FDI Attack

To defend against FDI attack on the cooperative control for voltage and reactive power of microgrids, a resilient control framework is developed in this section. The trust-based resilient control strategy relies on the local information to detect the misbehaving DGs, determines the malicious DGs

according to the common trust value obtained by the group decision-making mechanism, and eliminates the impacts of attack on the cooperative network through the recovery actions.

4.1. Misbehaving DG Detection Phase

(1) *Detection criteria*: The misbehavior of DG_i is defined as the abnormal update in cooperative control law (2) in the presence of FDI attack. The proposed detection method is based on the forward-backward consistency in updating Equation (2). Specifically, at iteration k, DG_i relies on its own information $\overline{x}_i(k)$ and its neighbors' information $\overline{x}_j(k)$ to obtain the forward update value $\overline{x}_i(k+1)$. Then, the following backward update rule is used to obtain the estimate of $\overline{x}_i(k)$:

$$\hat{x}_i(k) = \frac{1}{1-\varepsilon\sum_{j\in N_i} w_{ij}}(\overline{x}_i(k+1) - \varepsilon\sum_{j\in N_i} w_{ij}\overline{x}_j(k) - x_i(k+1) + x_i(k) \tag{15}$$

where $\hat{x}_i(k) = \left\{\hat{V}_i(k), \hat{Q}_i(k)\right\}$ is the estimated value of $\overline{x}_i(k)$. The backward update rule is derived from (2), and if there is no attack on DG_i, we should have $\hat{x}_i(k) = \overline{x}_i(k)$. Let $\theta_{ij}(k)$ denotes the detection result of DG_j to DG_i at iteration k, and can be expressed as:

$$\begin{cases} \theta_{ij}(k) = 1, & if\ \left\{\hat{V}_i(k), \hat{Q}_i(k)\right\} = \left\{\overline{V}_i(k), \overline{Q}_i(k)\right\} \\ \theta_{ij}(k) = 0, & otherwise \end{cases} \tag{16}$$

where $j \in N_i^+$, and $N_i^+ = \{i \cup N_i\}$ is the extended set of neighbors of DG_i.

(2) *Detection process*: According to Equation (16), the detection of attack on DG_i can be divided into the self-monitoring mechanism implemented by DG_i itself, and the neighbor-monitoring mechanism implemented by the neighbors of DG_i.

Self-monitoring mechanism: At iteration k, DG_i calculates $\overline{x}_i(k+1)$ according to the forward update rule (2). At iteration k+1, the estimated value $\hat{x}_i(k)$ is obtained by the backward update rule Equation (15). By comparing whether $\hat{x}_i(k)$ and $\overline{x}_i(k)$ are equal, DG_i is able to detect whether it is suffering from a FDI attack.

Neighbor-monitoring mechanism: Considering two neighboring DGs i and j, DG_j is responsible to monitor the misbehavior of DG_i. For DG_j to perform the estimation in (15), two-hop information is required, including the 1st-hop information set $\{\overline{x}_i(k+1),\ \overline{x}_i(k),\ x_i(k+1), x_i(k)\}$ from DG_i and the 2nd-hop information set $\{\overline{x}_s(k),\ s \in N_i\}$ from DG_i's neighbors. Then, DG_j compares the estimated value $\hat{x}_i(k)$ with the actual value $\overline{x}_i(k)$ to determine whether DG_i is experiencing an attack.

Remark 5. *In [33,34], only 1st-hop information is used to estimate the upper and lower bounds of state variables of DGs, and the state exceeding the bounds indicates the presence of attack. However, according to the analysis in Section 3, the false state even within the given bounds could affect the final operating point of microgrids. Although the additional 2nd-hop information increases a small amount of communication burden, it greatly improves the accuracy of intrusion detection. Moreover, by introducing the self-monitoring mechanism, the agent can realize self-diagnosis of its misbehavior, which also provides redundant information for the trust evaluation process.*

4.2. Trust Evaluation Phase

In multiagent network, trust index is defined as a confidence value that one agent puts on another agent [35]. Each DG maintains a trust index about its neighbors. $T_{ij}(k)$ represents DG_j's attitude about DG_i up to iteration k, where $j \in N_i^+$. In particular, $T_{ii}(k)$ denotes the trust level of DG_i to itself.

$T_{ij}(k) \in [0,1]$, 1 indicates the full trust level while 0 indicates the full distrust level. At each iteration, the trust index $T_{ij}(k)$ is updated as:

$$T_{ij}(k+1) = \alpha\theta_{ij}(k) + (1-\alpha)T_{ij}(k) \tag{17}$$

where $\alpha > 0$ is the sensitivity factor, which determines the change rate of $T_{ij}(k)$. It also guarantees that if the attack is not persistent after a while, the trust value will be recovered depending on the current observations. Initially, $T_{ij}(0)$ is set as 1 indicating that DG_j has full trust in DG_i. According to the detection result (16), if $\theta_{ij}(k) = 1$, then $T_{ij}(k+1) = 1$ indicates that DG_i is in the absence of attack; if $\theta_{ij}(k) = 0$, then $T_{ij}(k+1)$ starts to decrease which indicates that DG_i is suffering from attack.

In the traditional trust-based resilient system, if $T_{ij}(k)$ falls below a certain threshold T_L, then DG_i will be identified as malicious by its neighbors. However, this strategy is vulnerable to the colluding attack. The trust index can be manipulated by a colluder to keep the malicious DGs stay in the network or isolate the normal DGs from the network, which could cause instability of the microgrid in unforeseeable ways.

4.3. Malicious DGs Indentification Phase

While the abovementioned detection and trust evaluation process is effective for identifying the malicious DG under non-colluding attacks, it fails to consider the impacts of colluding attacks on the trust model. In general, colluding attacks may occur when two or more neighboring DGs are compromised. Figure 4 shows the colluding attack on the trust evaluation process. As illustrated in Figure 4, DG_j monitors DG_i's behavior and updates the trust index T_{ij} according to the information from DG_i. Considering that DG_j suffers from colluding attack, the attacker could tamper the trust index and distort DG_j's attitude about DG_i. The colluding DG_j can deliberately raise the trust index when the malicious behavior of DG_i has been detected. Thus, the false information will continue to propagate in the cooperative network. Another collusion is that DG_j intentionally reduce the trust index of an intact neighbor DG_i. Under such circumstances, the normal DG will be isolated from the network, which might result in overloads to cause disable or damage to other DGs.

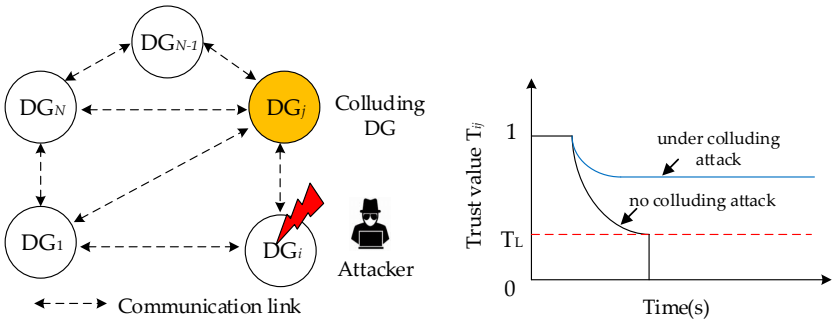

Figure 4. Illustration of colluding attack on the trust evaluation process.

To defend against a colluding attack, a group decision-making mechanism is introduced to settle conflicts arising from the dishonest trust index. The general idea is that for DG_j monitoring DG_i's misbehavior, other than only relying on its own local trust index to identify the malicious attack, DG_j receives the trust values from other neighbors of DG_i and utilizes them to form a collaborative opinion. To determine whether the targeted DG is malicious or not, at least half of its neighbors should share the same trust index. The similar group decision-making process have been used in other distributed systems, such as vehicular ad hoc networks [36] and wireless sensor networks [37]. The group decision-making process to identify the targeted DG as malicious or normal is presented as follows:

Step 1: At iteration k, DG_i sends its own trust index $T_{ii}(k)$ to the neighboring DGs, as well as relays all its neighbors' trust index $T_{ij}(k)$ $j \in N_i$ to the other neighbors.

Step 2: DG_j will receive two-hop neighbors' trust values about DG_i to form a trust index set $T_i(k) = \left\{T_{ij}(k), j \in N_i^+\right\}$. If at least half of the DGs in the trust index set share the common trust value $T_i^{com}(k)$, DG_j is able to determine whether DG_i is normal or malicious according to $T_i^{com}(k)$.

Step 3: If $T_i^{com}(k) \leq T_L$ where T_L is the isolation threshold, sets $T_{ij}(k) = 0$, DG_i will be identified as malicious and isolated from the network by DG_j.

Step 4: When the attacker terminates the attack and shifts to a sleep period, $T_{ij}(k)$ starts to increase. If $T_i^{com}(k) \geq T_H$ where T_H is the rejoining threshold, DG_i will be identified as normal by DG_j and rejoin the network.

4.4. Mitigation and Recovery Phase

To mitigate the adverse effects of FDI attack on the proposed cooperative control scheme of microgrid, it is necessary not only to isolate the malicious DGs from the network, but also add recovery information to eliminate the impacts of the injected false data. According to (3) and (14), the collective estimation error at iteration k can be expressed as:

$$Dev(k) = \sum_{i \in V} \overline{x}_i(k) - \sum_{i \in V} x_i(k) \tag{18}$$

since the initialization condition is chosen as $\overline{x}_i(0) = x_i(0)$ for all i, the equation $\sum_{i \in V} \overline{x}_i(k) = \sum_{i \in V} x_i(k)$ should always hold true in the iteration process. The collective estimation error $Dev(k)$ should equal to zero in the absence of FDI attack. Therefore, to maintain the correct average estimates under attack, it is crucial to protect the collective estimation error from the injected false data.

To describe the mitigation and recovery process, the neighboring DG_i and DG_j are still used as the example and the general idea is explained as follows:

(1) Discarding information mechanism.

At k_0 iteration, DG_j detects DG_i's misbehavior and the common trust value $T_i^{com}(k)$ starts to decrease. The average estimates information sent from DG_i will be discarded. Correspondingly, the updating rule (2) for DG_j changes to:

$$\overline{x}_j(k+1) = \overline{x}_j(k) + \varepsilon \sum_{s \in N_j}^{s \neq i} w_{js}\left(\overline{x}_s(k) - \overline{x}_j(k)\right) + x_j(k+1) - x_j(k),\ j \in N_i \tag{19}$$

The above discarding information mechanism can prevent the propagation of false data in the cooperative network. From k_0 iteration, DG_j will update according to (19) until the following recovery action is activated.

(2) Recovery action for transient disturbance.

During the iteration process, the updating rule (2) may be affected by the transient faults or unmodeled dynamics. In this case, DG_i only misbehaves for a limited number of iterations. Although the common trust value $T_i^{com}(k)$ decreases, it is still above the isolation threshold T_L. At a certain iteration k_1, the common trust value increase above T_H, DG_i will be identified as a normal DG and welcomed to rejoin the calculation process. DG_i resends the average estimate and measurement information about k_0 iteration to is neighbors, and the recovery action can be expressed as:

$$\begin{cases} \overline{x}_j(k_1+1) = \overline{x}_j(k_1) + \varepsilon \sum\limits_{s\in N_j}^{s\neq i} w_{js}\Big(\overline{x}_s(k_1) - \overline{x}_j(k_1)\Big) + x_j(k_1+1) - x_j(k_1) + v_j,\ j \in N_i \\ \overline{x}_i(k_1+1) = \overline{x}_i(k_0) + \varepsilon \sum\limits_{j\in N_i} w_{ij}\Big(\overline{x}_j(k_1) - \overline{x}_j(k_0)\Big) + x_i(k_1+1) - x_i(k_0) \\ v_j = \varepsilon w_{ji}\Big(\overline{x}_i(k_0) - \overline{x}_j(k_1)\Big) \end{cases} \tag{20}$$

where v_j is the recovery information added to the neighbors of DG_i. From iteration k_1+1, all DGs are considered as normal and update according to (2).

Theorem 1. *In the transient disturbance scenario, with the proposed recovery action Equation (20), the average estimates can be ensured to converge to the correct average value for all normal DGs, i.e.,* $\lim\limits_{k\to\infty} \overline{x}_s(k) = \frac{1}{N} \lim\limits_{k\to\infty} \sum\limits_{s\in V_{norm}} x_i(k)$*, where* $V_{norm} = V$ *is the set of normal DGs.*

Proof. At iteration k_0, DG_i is affected by transient disturbance and its broadcast information is rejected by its neighbors according to the discarding mechanism Equation (19). Since the cooperative network is under no attack until iteration $k = k_0 - 1$, according to (2) we have:

$$\sum_{s\in V}^{s\neq i} \overline{x}_s(k_0) + \overline{x}_i(k_0) = \sum_{s\in V}^{s\neq i} x_s(k_0) + x_i(k_0) \tag{21}$$

Rearranging Equation (21) and the following equation holds:

$$\sum_{s\in V}^{s\neq i} \overline{x}_s(k_0) - \sum_{s\in V}^{s\neq i} x_s(k_0) = x_i(k_0) - \overline{x}_i(k_0) \tag{22}$$

From iteration k_0 to $k_1 - 1$, the normal neighbors of DG_i update according to Equation (19), the other normal DGs in the cooperative network update according to (2). The set of normal DGs is $V_{norm} = \{V \backslash i\}$. By summing $\overline{x}_s(k)$ over the normal DGs, we have:

$$\sum_{s\in V}^{s\neq i} \overline{x}_s(k+1) = \sum_{s\in V}^{s\neq i} \overline{x}_s(k) + \sum_{s\in V}^{s\neq i} x_s(k+1) - \sum_{s\in V}^{s\neq i} x_s(k), k_0 \le k \le k_1 - 1 \tag{23}$$

Combining Equations (22) and (23), the collective estimation error from k_0 to $k_1 - 1$ can be obtained:

$$Dev(k+1) = \sum_{s\in V}^{s\neq i} \overline{x}_s(k+1) - \sum_{s\in V}^{s\neq i} x_s(k+1) = x_i(k_0) - \overline{x}_i(k_0), k_0 \le k \le k_1 - 1 \tag{24}$$

The above equation shows that the collective estimation error of normal DGs from iteration $k_0 + 1$ to k_1 is determined by the discarding information mechanism at k_0 iteration.

At iteration $k = k_1$, DG_i is re-identified as normal by its neighbors and resends the correct information which should be sent at iteration k_0. Since the set of normal DGs become $V_{norm} = \{V\}$, with the recovery action Equation (20) at iteration k_1, the summation of average estimates over all DGs can be expressed as:

$$\sum_{s\in V} \overline{x}_s(k_1+1) = \sum_{s\in V} x_s(k_1+1) + \Big(\sum_{s\in V}^{s\neq i} \overline{x}_s(k_1) + \overline{x}_s(k_0)\Big) - \Big(\sum_{s\in V}^{s\neq i} \overline{x}_s(k_1) - \overline{x}_s(k_0)\Big) \tag{25}$$

Combining Equations (24) and (25), the following equation holds:

$$Dev(k+1) = \sum_{s\in V} \overline{x}_s(k+1) - \sum_{s\in V} x_s(k+1) = 0, k \geq k_1 \tag{26}$$

The above equation shows that from iteration k_1+1, the collective estimation error becomes zero due to the proposed recovery action Equation (20). Thus, all normal DGs update according to the dynamic consensus Algorithm (2), and the correct average value of voltages and reactive power can be obtained, i.e., $\lim_{k\to\infty} \overline{x}_s(k) = \frac{1}{N} \lim_{k\to\infty} \sum_{s\in V_{norm}} x_i(k)$, $V_{norm} = V$. □

Remark 6. *When* DG_i *is re-identified as normal, it needs to resend the average estimate* $\overline{x}_i(k_0)$ *and measurement information* $x_i(k_0)$*about*k_0 *iteration. The proposed recovery action Equation (20) requires that the control unit of* DG_i *has certain storage capacity. Since* $\overline{x}_i(k_0)$ *can be calculated by the information set* $\{\overline{x}_i(k_0-1),\ x_i(k_0-1), \overline{x}_j(k_0-1), j \in N_i\}$ *according to (2),* DG_i *only needs to store the average estimate, measurement and its neighbors' broadcast information in the last iteration process. Although it increases the storage burden of control unit, this mechanism considerably improves the security and robustness of the microgrid system.*

(3) Recovery action for continuous FDI attack.

Considering that DG_j detects DG_i's misbehavior from iteration k_0, and the common trust value $T_i^{com}(k)$ falls below the isolation threshold T_L at a certain iteration k_2. Since then, DG_i is identified as malicious by its neighbors and isolated from the network. Thus, the set of normal DGs becomes $V_{norm} = \{V \backslash i\}$. To eliminate the adverse effects of FDI attack on the proposed secondary control scheme, the recovery action is taken by the neighbors of DG_i at iteration k_2, and is given by:

$$\begin{cases} \overline{x}_j(k_2+1) = \overline{x}_j(k_2) + \varepsilon \sum\limits_{s\in N_j}^{s\neq i} w_{js}\left(\overline{x}_s(k_2) - \overline{x}_j(k_2)\right) + x_j(k_2+1) - x_j(k_2) + v_j,\ j \in N_i \\ v_j = \frac{1}{|N_i|}\left(\overline{x}_i(k_0) - x_i(k_0)\right) \end{cases} \tag{27}$$

where v_j is the recovery information when DG_i is isolated from the cooperative network.

From iteration k_2+1, the remaining DGs in the microgrid are considered as normal and update according to (2). As stated in Section 3, the attacker will terminate the attack activity and shift to a sleep period to avoid being exposed to the intrusion detection system. When the attack is cleared, DG_i can detect its update return to normal by the self-monitoring mechanism and the trust value starts to increase. At the same time, the neighbors of DG_i will receive the average estimates and measurement information to perform neighbor-monitoring mechanism. When the common trust value increase above the rejoining threshold T_H at a certain iteration k_3, DG_i will be re-identified as normal and rejoin the cooperative network. The recovery action for DG_i rejoining the network is expressed as:

$$\begin{cases} \overline{x}_j(k_3+1) = \overline{x}_j(k_3) + \varepsilon \sum\limits_{s\in N_j}^{s\neq i} w_{js}\left(\overline{x}_s(k_3) - \overline{x}_j(k_3)\right) + x_j(k_3+1) - x_j(k_3) + v_j,\ j \in N_i \\ \overline{x}_i(k_3+1) = \overline{x}_i(k_0) + \varepsilon \sum\limits_{j\in N_i} w_{ij}\left(\overline{x}_j(k_3) - \overline{x}_i(k_0)\right) + x_i(k_3+1) - x_i(k_0) \\ v_j = -\frac{1}{|N_i|}\left(\overline{x}_i(k_0) - x_i(k_0)\right) + \varepsilon w_{ji}\left(\overline{x}_i(k_0) - \overline{x}_j(k_3)\right) \end{cases} \tag{28}$$

where v_j is the recovery information when DG_i rejoins the cooperative network.

Theorem 2. *In the continuous FDI attack scenario, when the malicious* DG_i *is isolated, the average estimates can be ensured to converge to the correct average value for the remaining normal DGs with the proposed recovery action Equation (27), i.e.,* $\lim_{k\to\infty} \overline{x}_s(k) = \frac{1}{N} \lim_{k\to\infty} \sum_{s\in V_{norm}} x_i(k)$*, where* $V_{norm} = \{V \backslash i\}$*. When the attack is over,*

DG_i *is re-identified as normal and rejoins the cooperative network, the proposed recovery action Equation (28) is able to ensure all normal DGs to converge to the correct average value, i.e.,* $\lim_{k\to\infty}\overline{x}_s(k) = \frac{1}{N}\lim_{k\to\infty}\sum_{s\in V_{norm}}x_i(k)$, *where* $V_{norm} = V$.

Proof. At iteration k_2, the set of normal DGs is $V_{norm} = \{V\backslash i\}$. The neighbors of DG_i update according to Equation (27), the other normal DGs update according to (2). With the recovery action Equation (27), the summation of $\overline{x}_s(k)$ over the normal DGs at iteration k_2 is:

$$\sum_{s\in V}^{s\neq i}\overline{x}_s(k_2+1) = \sum_{s\in V}^{s\neq i}\overline{x}_s(k_2) + \sum_{s\in V}^{s\neq i}x_s(k_2+1) - \sum_{s\in V}^{s\neq i}x_s(k_2) + \frac{1}{|N_i|}(\overline{x}_i(k_0) - x_i(k_0)) \tag{29}$$

Combining Equations (29) and (24), the collective estimation error of the remaining normal DGs is:

$$Dev(k+1) = \sum_{s\in V}^{s\neq i}\overline{x}_s(k_2+1) - \sum_{s\in V}^{s\neq i}x_s(k_2+1) = 0, k \geq k_2 \tag{30}$$

From iteration k_2+1, all the remaining normal DGs update according to (2). It is easy to find that the collective estimation error of the remaining normal DG keeps zero from iteration k_2. Thus, the correct average estimate of voltage and reactive power can be obtained by the remaining normal DGs, i.e., $\lim_{k\to\infty}\overline{x}_s(k) = \frac{1}{N}\lim_{k\to\infty}\sum_{s\in V_{norm}}x_i(k)$, $V_{norm} = \{V\backslash i\}$.

After the attacker terminates the attack activity, DG_i will be re-identified as normal and rejoins the cooperative network at iteration k_3. The set of normal DGs becomes $V_{norm} = V$. Combing Equations (24) and (29) and the recovery action Equation (20), the collective estimation error of the normal DGs can be given as:

$$Dev(k+1) = \sum_{s\in V}\overline{x}_s(k+1) - \sum_{s\in V}x_s(k+1) = 0, k \geq k_3 \tag{31}$$

The above equation shows that from iteration k_3+1, the collective estimation error becomes zero due to the proposed recovery action Equation (28). Therefore, when the attacker shifts to a sleep period, the correct average estimates can be obtained for all DGs with the recovery action Equation (28), i.e., $\lim_{k\to\infty}\overline{x}_s(k) = \frac{1}{N}\lim_{k\to\infty}\sum_{s\in V_{norm}}x_i(k)$, $V_{norm} = V$. □

Remark 7. *When* DG_i *is identified as malicious DG, the outgoing communication links of* G_i *will be deactivated. This isolation operation may lead to the disconnection of the communication topology, which makes the remaining normal DGs unable to reach consensus. To prevent this condition, adding redundant communication links or rely nodes can improve the connectivity of the communication network. When the attacker terminates the attack activity, the deactivated links will be restored back. The connectivity of the communication network can be restored, thus all DGs can update according to the dynamic consensus protocol (2).*

For the sake of clarity, the trust-based resilient control framework for voltage and reactive power of an islanded microgrid is summarized as Algorithm 1.

Algorithm 1. Trust-based resilient control framework for voltage and reactive power control.

At iteration k

1. **Misbehavior detection:** DG_j ($j \in N_i^+$) detects DG_i's misbehavior according to (15).
2. **Trust evaluation:** DG_j ($j \in N_i^+$) updates the trust index $T_{ij}(k)$ according to (17).
3. **Group decision-making:** DG_j relies on the trust indexes from the other neighbors of DG_i to form a collaborative opinion $T_i^{com}(k)$.
4. **Information discarding:** At a certain iteration k_0, if the common trust value $T_i^{com}(k)$ starts to decrease, DG_j discards the information from DG_i and updates according to (19).
5. DG_j compares $T_i^{com}(k)$ with the isolation threshold T_L. If $T_i^{com}(k) \geq T_L$, go to step 6; otherwise, go to step 7.

// **Transient disturbance scenario** //

6. **Recovery action for disturbance:** If $T_i^{com}(k)$ increase above T_H (i.e., $T_i^{com}(k) \geq T_H$), DG_j asks DG_i to resend information about k_0 iteration and takes recovery action according to (20), go to step 10.

// **Continuous FDI attack scenario** //

7. **Recovery action for isolation:** DG_j identifies DG_i as a malicious DG and sets $T_{ij}(k) = 0$. DG_i is isolated from the cooperative network, the adverse effect of DG_i is eliminated by recovery action (27).
8. DG_i performs self-monitoring to detect whether the attack is over. If $T_{ii}(k)$ starts to increase, the deactivated links from is restored back. DG_j can receive information from DG_i to perform neighbor-monitoring.
9. **Recovery action for rejoining:** If $T_i^{com}(k)$ increases above T_H, DG_j re-identifies DG_i as a normal DG. DG_i rejoins the cooperative network, both DG_j and DG_i take recovery action according to (28).
10. Repeats for $k = k + 1$.

5. Simulation Results and Discussion

In this section, the effectiveness of the proposed trust-based resilient control scheme for voltage restoration and reactive power sharing of an islanded microgrid is verified. Figure 5 shows the microgrid test system.

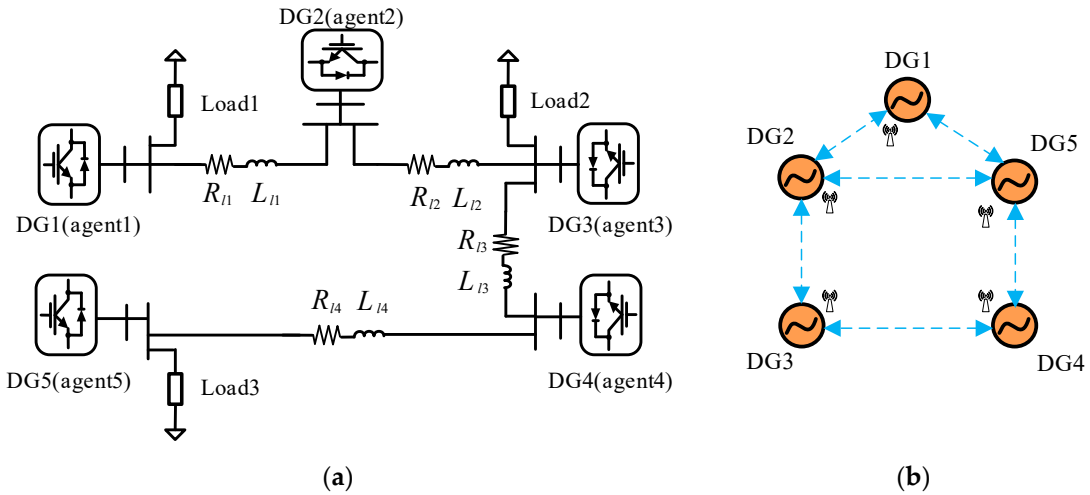

Figure 5. Islanded microgrid test system: (**a**) Physical model; (**b**) Communication topology.

As illustrated in Figure 5a, a 380/50 Hz islanded microgrid consisting of five DGs and three loads is built using MATLAB/Simulink toolbox. The lines parameters, loads and related control parameters of the microgrid test system are given in Table 1, in which K_{PV} and K_{IV} are respectively the proportional and integral gains of the PI voltage control loop in the primary control, while K_{PC} and K_{IC} are respectively the proportional and integral gains of the PI current control loop in the primary control. The communication network in secondary control level is shown in Figure 5b. As seen, the communication topology satisfies the condition that being connected. To satisfy the

real-time information transmission requirement, the sampling period is set to 10 ms. In order to test the performance of the proposed resilient control scheme, different scenarios are tested, such as transient disturbance, continuous FDI attack and colluding attacks. It should be noted that each event in the abovementioned scenarios are separated to provide clear understanding.

Table 1. Parameter values for simulation.

DG1 & DG2 (25 kW, 15 kVar)		**DG3 & DG4 & DG5 (20 kW, 12 kVar)**	
$R^f = 0.1\ \Omega$	$L^f = 1.35$ mH	$R^f = 0.1\ \Omega$	$L^f = 1.35$ mH
$R^c = 0.03\ \Omega$	$L^c = 0.35$ mH	$R^c = 0.03\ \Omega$	$L^c = 0.35$ mH
$m^P = 9.4 \times 10^{-5}$	$n^Q = 1.3 \times 10^{-3}$	$m^P = 12.5 \times 10^{-5}$	$n^Q = 1.5 \times 10^{-3}$
$K_{PV} = 0.1$	$K_{IV} = 420$	$K_{PV} = 0.05$	$K_{IV} = 390$
$K_{PC} = 15$	$K_{IC} = 20,000$	$K_{PC} = 10.5$	$K_{IC} = 16,000$
Line 1 & Line 3		**Line 2& Line 4**	
$R_{l1} = 0.23$	$L_{l1} = 0.318$ mH	$R_{l2} = 0.35$	$L_{l1} = 1.847$ mH
Load 1	**Load 2**	**Load 3**	
12kW + 10 kVar	15 kW + 5 kVar	6 kW + 6 kVar	
Secondary Control Parameters			
$K_{PV}^{AVE} = 0.001$	$K_{IV}^{AVE} = 10$	$K_{PQ}^{AVE} = 0.0001$	$K_{IQ}^{AVE} = 0.03$ $\varepsilon = 0.1$
Trust Evaluation Parameters			
$\alpha = 0.08$	$T_L = 0.2$	$T_H = 0.9$	

5.1. Transient Disturbance Scenario

In order to verify the effectiveness of the proposed resilient secondary control scheme under transient disturbance, the simulation process is designed as follows: (1) From t = 0 s, the microgrid works in islanded mode and only the primary control is activated for all five DGs. (2) At t = 0.5 s, the proposed secondary control scheme is applied. (3) At t = 0.7 s, the transient disturbance signals $f_{1,V}^a(k) = rand\ (-0.5,\ 0.5)$ and $f_{1,Q}^a(k) = rand\ (-500,\ 500)$ are injected into DG1 according to Equation (8). Then, the disturbance is cleared at t = 0.8s. (4) At t = 2 s, Load1 is reduced by the amount of 4kVar. The simulation results are shown in Figure 6.

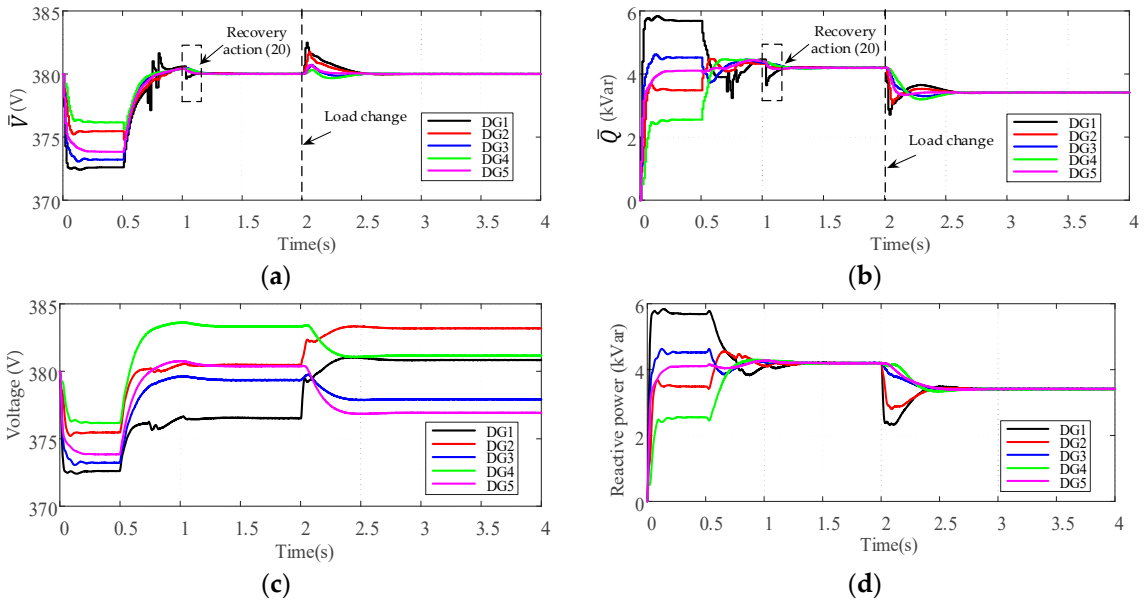

Figure 6. *Cont.*

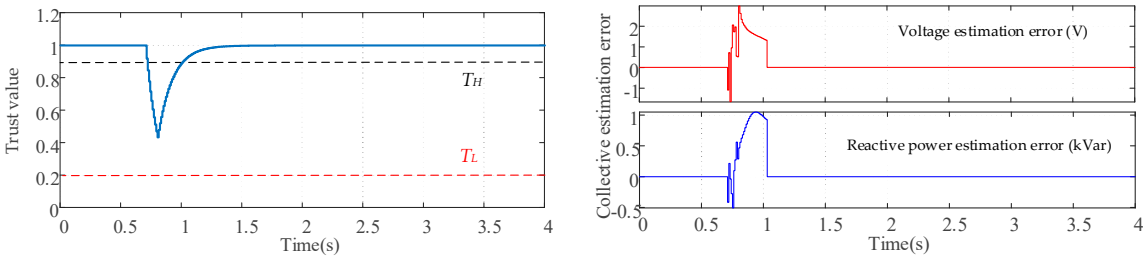

(**e**) (**f**)

Figure 6. Performance of the proposed control scheme under transient disturbance: (**a**) Average voltage estimates; (**b**) Average reactive power estimates; (**c**) Voltages of DGs; (**d**) Reactive power of DGs. (**e**) Common trust value of DG1; (**f**) Collective estimation error.

Figure 6a,b show the evolutions of average estimates $\overline{V}(k)$ and $\overline{Q}(k)$ under transient disturbance and load changes. Figure 6c,d show the evolutions of DG output voltages and reactive power. Figure 6e shows the common trust value of DG1 which obtained by the proposed group decision-making process. Figure 6f shows the deviations of the collective estimation error which is calculated according to Equation (18). As can be seen that when the broadcast information $\overline{V}_1(k)$ and $\overline{Q}_1(k)$ of DG1 are affected by the transient disturbance, the common trust value of DG1 starts to decrease from t =0.7 s. Meanwhile, the neighbors of DG1 activate the discarding information mechanism, which prevents the propagation of the false data in the secondary control level. The collective estimation error of overall DGs is not equal to zero due to the presence of disturbance. When the disturbance is removed at t = 0.8 s, the common trust value of DG1 starts to increase. At t = 1.02 s the common trust value increases above the rejoining threshold $T_H = 0.9$, DG1 is re-identified as the normal DG by its neighbors. The recovery action according to Equation (20) is taken by DG1 and its neighbors. Consequently, the collective estimation error becomes zero due to the recovery action, which ensures the correct estimation of average voltage and reactive power. As seen in Figure 6c,d, the proposed resilient control scheme is able to restore the average voltages to the rated value 380V while maintaining the accurately reactive power sharing under transient disturbance. Furthermore, when the load changes at t = 2 s, the common trust value of DG1 is not affected by such change. It can be concluded that our approach can successfully differentiate between the false data injection and the normal load change.

To further explain the necessity of the proposed recovery action Equation (20), a case study is also done only with the discarding information mechanism. As can be seen in Figure 7a,b, although the discarding information mechanism prevents the propagation of false data, the average estimates $\overline{V}(k)$ and $\overline{Q}(k)$ cannot converge to the correct values without the recovery action Equation (20). Due to the adverse effects of false data, $\overline{V}(k)$ converges to the incorrect stable point 380.55 V while $\overline{Q}(k)$ abnormally increases from 4.2 kVar to 4.39 kVar. From Figure 7f, it can be easily seen that the collective estimation error is still not equal to zero even when the disturbance is cleared and DG1 rejoins the cooperative network at t = 1.02 s. It is concluded that the control objectives of average voltage restoration and reactive power sharing cannot be achieved without the recovery action Equation (20). Under such circumstance, the false data may lead to the abnormal changes of DGs' output voltages and the circulating currents between different DGs which disrupts the stability and performance of the islanded microgrid.

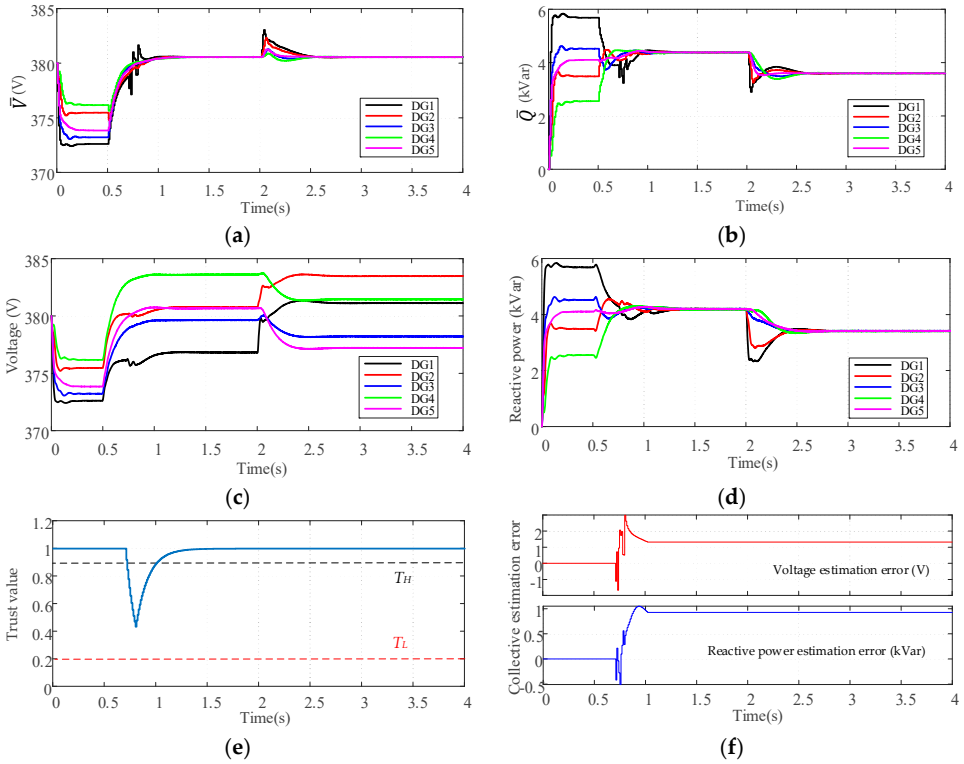

Figure 7. Performance of the control scheme only with the discarding information mechanism: (**a**) Average voltage estimates; (**b**) Average reactive power estimates; (**c**) Voltages of DGs; (**d**) Reactive power of DGs. (**e**) Common trust value of DG1; (**f**) Collective estimation error.

5.2. Continuous FDI Attack Scenario

In this case study, the effectiveness of the proposed resilient control scheme under continuous FDI attack is verified. At $t = 0.7$ s, the attack signals $f^a_{1,V}(k) = 0.5$ and $f^a_{1,Q}(k) = -200$ are injected into DG1 according to Equation (8). Then, the injected false data is removed by the attacker at $t = 2$ s and the system returns to secure. Other simulation process is similar with the case study under transient disturbance. The simulation results are demonstrated in Figure 8.

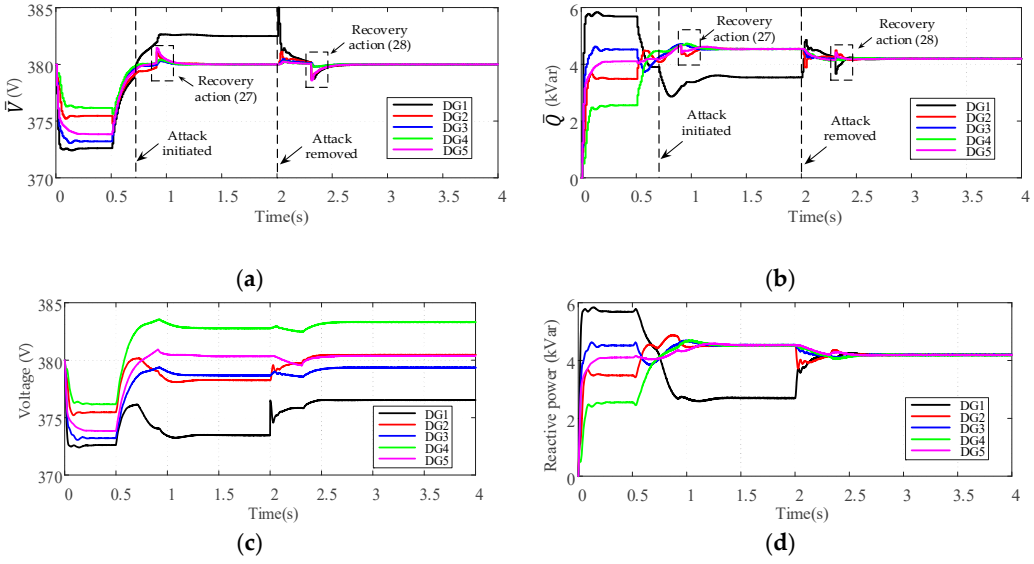

Figure 8. *Cont.*

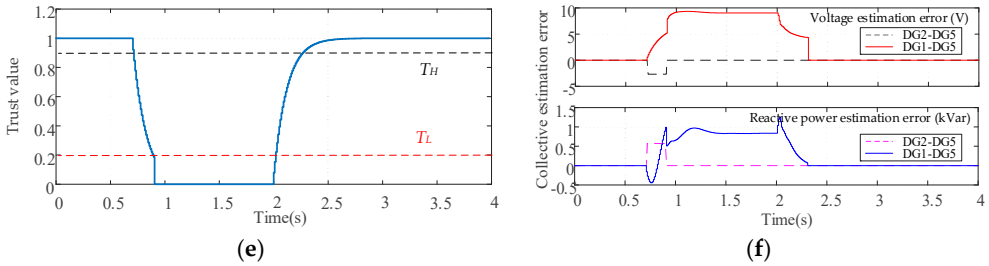

(**e**) (**f**)

Figure 8. Performance of the proposed control scheme under continuous FDI attack: (**a**) Average voltage estimates; (**b**) Average reactive power estimates; (**c**) Voltages of DGs; (**d**) Reactive power of DGs. (**e**) Common trust value of DG1; (**f**) Collective estimation error.

Figure 8 shows the resilience of the proposed control scheme in the continuous FDI attack scenario. As illustrated in Figure 8e, when the attacker starts to inject false data in DG1, the common trust value of DG1 keeps decreasing. When the common trust value reaches the isolation threshold $T_L = 0.2$ at $t = 0.9$ s, the outgoing communication links of DG1 are deactivated and the recovery action is taken by the neighbors of DG1 according to Equation (27). It can be seen from Figure 8f that, the collective estimation error of the remaining normal DGs (DG2 to DG5) becomes zero after the recovery action Equation (27). Consequently, the remaining normal DGs can still converge to the desired stable point, without considering the attacked DG1 in the operation, which is illustrated in Figure 8a,b. After the attacker terminates the attack activity at $t = 2$ s, the common trust value of DG1 starts to increase. When the common trust value increases above the rejoining threshold $T_H = 0.9$ at $t = 2.31$ s, DG1 is re-identified as the normal DG and the recovery action is taken by DG1 and its neighbors according to Equation (28). At that moment, we can see from Figure 8f that the collective estimation error of all normal DGs (DG1 to DG5) becomes zero due to the effects of the recovery action Equation (28). Since all DGs are considered as normal, the correct average estimates of voltages and reactive power can be gradually obtained in a distributed manner, as shown in Figure 8a,b. Thus, the control objectives of average voltage restoration and reactive power sharing are not affected by the continuous FDI attack with our control scheme, which can be seen from Figure 8c,d.

A case study is also conducted to show the effectiveness and necessity of the proposed recovery actions Equations (27) and (28). Figure 9 shows the evolution of the variables under continuous FDI attack only with the discarding information mechanism. As shown in Figure 9a, without the recovery action Equation (27), the average estimate $\overline{V}(k)$ obtained by the remaining normal DGs converges to the incorrect stable point 380.45 V even after the compromised DG1 is isolated from $t = 0.9$ s. And after the false data is removed from $t = 2$ s, the average estimate $\overline{V}(k)$ converges to 380.50 V which causes the abnormal voltages rise of all DGs, as shown in Figure 9c. The similar abnormal changes in the average estimate $\overline{Q}(k)$ and DGs output reactive power also can be seen from Figure 9b,d. It can be easily seen from Figure 9f that, without the recovery action Equation (27), the collective estimation error of the remaining normal DGs is not equal to zero although DG1 is isolated from the network. When DG1 rejoins the network at $t = 2.31$ s, the collective estimation error is still not equal to zero without the recovery action Equation (28). It can be concluded that the correct average estimates cannot be obtained without the recovery actions Equations (27) and (28), which adversely affects the performance of the microgrid system in the continuous FDI attack scenario.

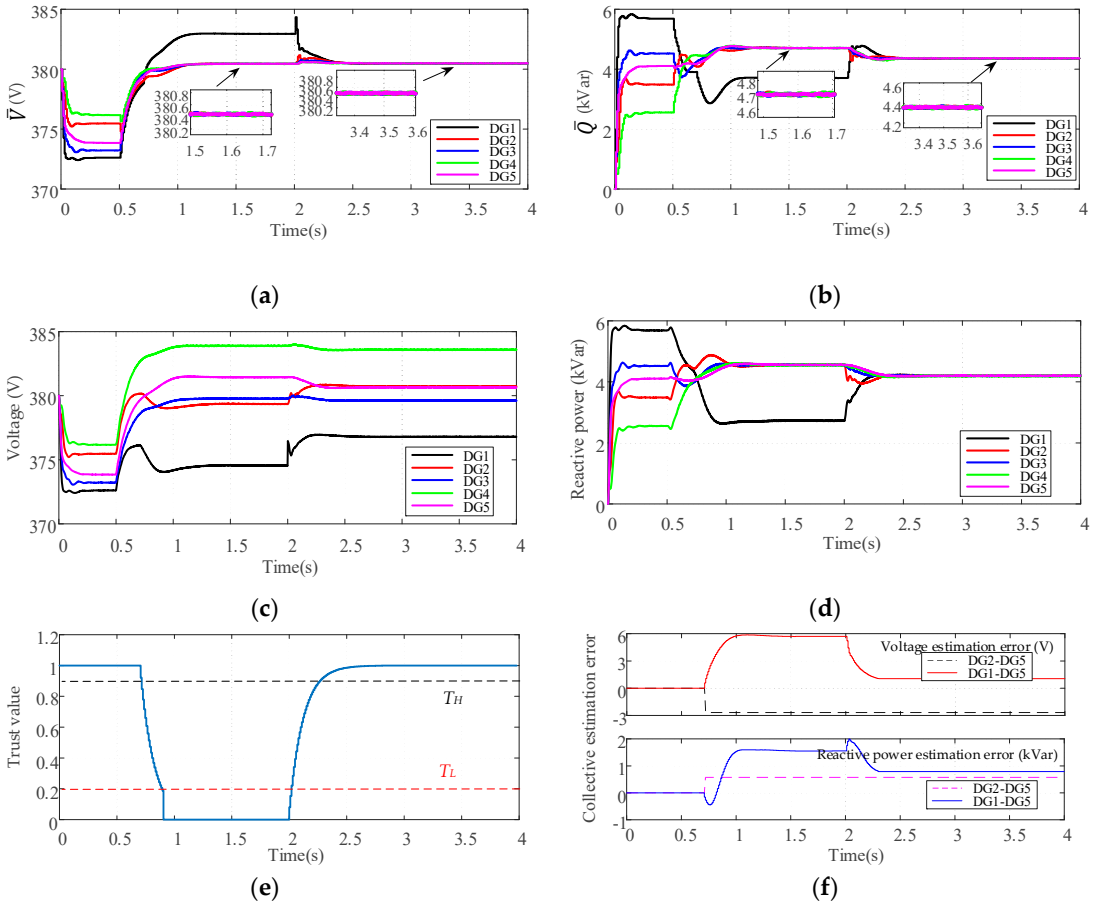

Figure 9. Performance of the control scheme only with the discarding information mechanism: (**a**) Average voltage estimates; (**b**) Average reactive power estimates; (**c**) Voltages of DGs; (**d**) Reactive power of DGs. (**e**) Common trust value of DG1; (**f**) Collective estimation error.

5.3. Multiple Attakers and Colluding Attack Scenario

In this case study, DG1 and DG4 are assumed to be attacked to test the robustness of the proposed control scheme in the multiple attackers scenario. At $t = 0.7$ s, the attack signals $f^a_{1,V}(k) = -0.3$ and $f^a_{1,Q}(k) = 100$ are injected into DG1, while the attack signals $f^a_{4,V}(k) = 0.3$ and $f^a_{4,Q}(k) = -100$ are injected into DG4, respectively. At $t = 2.5$ s, all the attack signals are cleared. It can be seen that the cumulative effect of the attack signals is zero, which satisfies the condition given by Equation (13). Thus, this case study also can verify the effectiveness of the proposed control scheme under probing attack. Furthermore, to valid the resistance of the proposed approach to colluding attack, the trust index $T_{43}(k)$ which represents DG3's attitude about DG4 is manipulated by the colluding attacker from $t = 0.8$ s. The simulation results are illustrated in Figure 10.

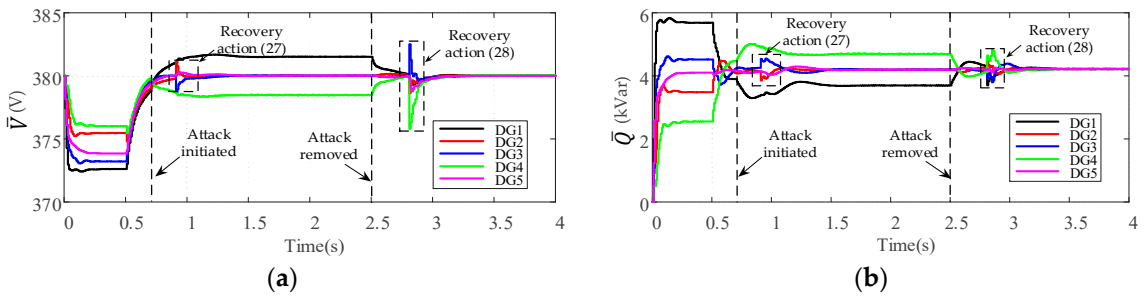

Figure 10. *Cont.*

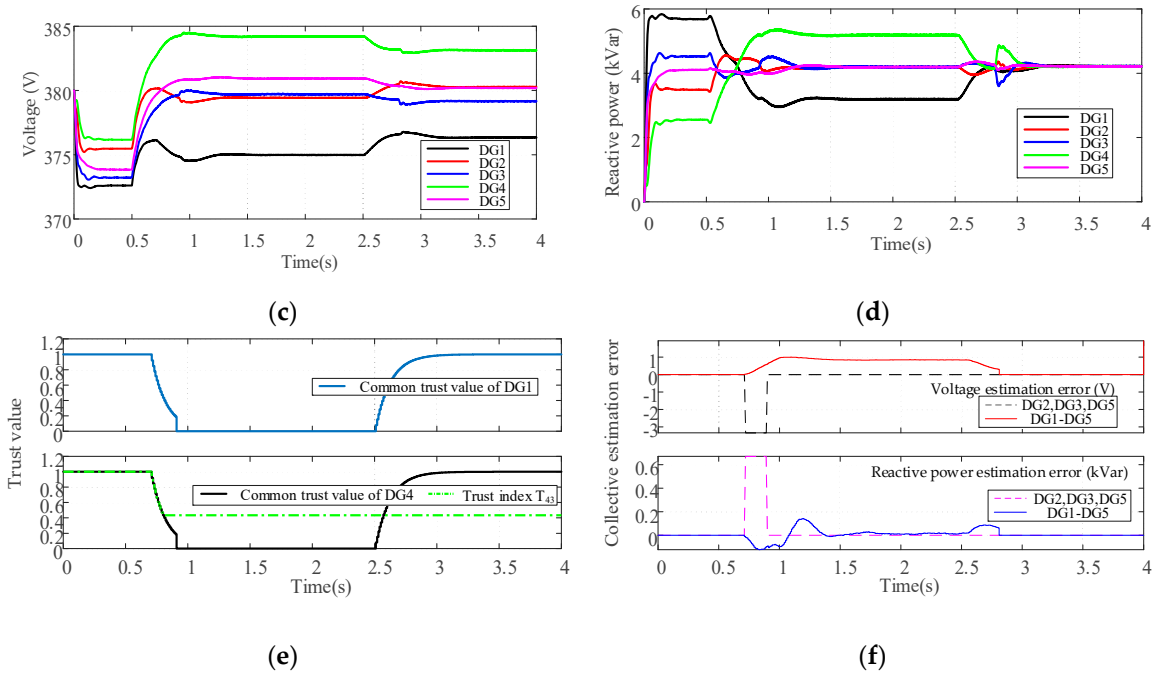

Figure 10. Performance of the proposed control scheme with multiple attackers and colluding attack: (**a**) Average voltage estimates; (**b**) Average reactive power estimates; (**c**) Voltages of DGs; (**d**) Reactive power of DGs. (**e**) Common trust values of DG1 and DG4; (**f**) Collective estimation error.

As shown in Figure 10a,b, the average voltage and reactive power estimates of the remaining normal DGs (DG2, DG3 and DG5) can still converge to the desired consensus values under the effect of the recovery action Equation (27), when DG1 and DG4 are attacked from t = 0.7 s. After the attackers terminate the attack activity at t = 2 s, all DGs are considered as normal, and the recovery action Equation (28) makes the average estimates of all normal DGs converge to the correct values. Consequently, from Figure 10c,b we can see that the control objectives of average voltage restoration and reactive power sharing can be achieved with the proposed control scheme. From Figure 10e, it can be seen that both malicious DGs are detected by the trust-based detection mechanism, as the common trust values of DG1 and DG4 continue to drop from t = 0.7 s. It should be noted that although DG3's attitude toward DG4 are manipulated by the colluding attacker from t = 0.8 s, the group decision-making mechanism is able to ensure the correct common trust value of DG4. According to the common trust value, DG4 is identified as the malicious DG by its neighbor at t = 0.9 s, and the adverse impact of false data can be eliminated by the recovery action Equation (27) when DG4 is isolated from the cooperative network. After the attack is cleared at t = 2.5 s, the common trust values of DG1 and DG4 keep increasing. Then, DG1 and DG4 are identified as normal DGs when the common trust values increase above the rejoining threshold. As shown in Figure 10f, the deviation of the collective estimation error of DG2, DG3 and DG5 starts from t = 0.7 s, because the broadcast information of DG1 and DG4 is discarded by their neighbors. Later, when DG1 and DG4 are isolated from the network, the collective estimation error of DG2, DG3 and DG5 becomes zero due to the recovery action Equation (27). It also can be seen from Figure 10f that, when the attack is removed and all DGs are considered as normal, the recovery action Equation (28) can successfully correct the collective estimation error of all DGs.

5.4. Impacts of Parameter Selection on the Performance of Resilient Control Scheme

In this subsection, the impacts of the parameter selection on the performance of the proposed control scheme are investigated. It is assumed that the attack signals $f^a_{1,V}(k) = 0.5$ and $f^a_{1,Q}(k) = -200$ are injected into DG1 according to Equation (8) from t = 0.7 s. Then, the attack is removed at t = 2.5 s.

Figure 11 shows the impacts of sensitivity factor α on the common trust value of DG1. Figures 12 and 13 show the evolutions of DG1's common trust value and the collective estimation error under different isolation threshold T_L and rejoining threshold T_H.

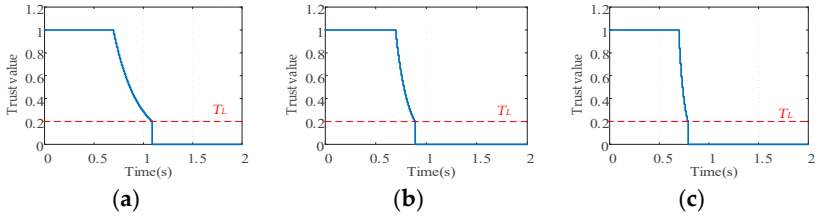

Figure 11. Impacts of sensitivity factor α on the common trust value of DG1: (**a**) $\alpha = 0.04$; (**b**) $\alpha = 0.08$; (**c**) $\alpha = 0.16$.

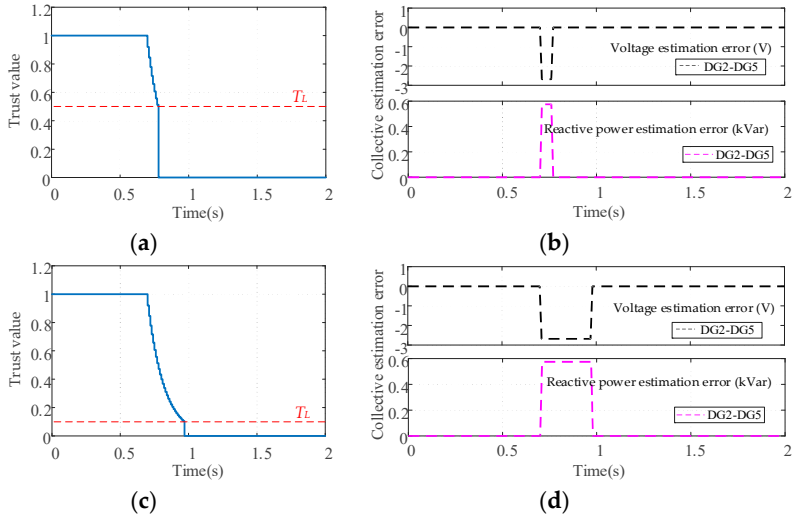

Figure 12. The impacts of isolation threshold T_L on the collective estimation error: (**a**) DG1's common trust value under $T_L = 0.5$; (**b**) Collective estimation error of DG2 to DG5 under $T_L = 0.5$; (**c**) DG1's common trust value under $T_L = 0.1$; (**d**) Collective estimation error of DG2 to DG5 under $T_L = 0.1$.

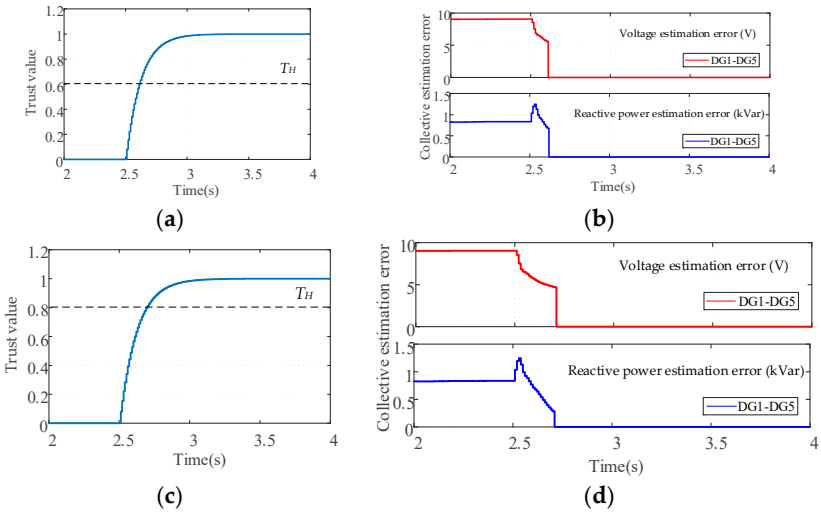

Figure 13. The impacts of rejoining threshold T_H on the collective estimation error: (**a**) DG1's common trust value under $T_H = 0.6$; (**b**) Collective estimation error of all DGs under $T_H = 0.6$; (**c**) DG1's common trust value under $T_H = 0.8$; (**d**) Collective estimation error of all DGs under $T_H = 0.8$.

As can be seen from Figure 11, with the increase of sensitivity factor α, the decline rate of common trust value will increase. Since the attacked DG will be isolated from the network when the common trust value drops below the isolation threshold, a smaller sensitivity factor can improve the tolerance of the proposed control scheme to the transient disturbance before a DG is identified as malicious. However, if the sensitivity factor is too small, the neighbors will spend more time to determine the malicious DG, which reduces the quickness of the detection process.

Figures 12 and 13 show the evolutions of the collective estimation error under different isolation threshold T_L and rejoining threshold T_H where the sensitivity factor α is chosen as 0.08. From Figure 12, we can see that the deviation of the collective estimation error of DG2 to DG5 starts from t = 0.7 s due to the discarding information mechanism. When the common trust value drops below the isolation threshold T_L, the collective estimation error will be corrected by the recovery action Equation (27). It can be seen that the isolation threshold only affects the duration of the deviation, while the magnitudes of deviation are the same. From Figure 13, we can see that after the attack is cleared at t = 2.5 s, the deviation of the collective estimation error of all normal DGs will be corrected by the recovery action Equation (28) when the common trust value increases above the rejoining threshold T_H. Although a smaller T_H can reduce the duration of deviation of collective estimation error, it also increases the risk that an attacked DG will be misidentified as a normal one. It can be concluded that the smaller isolation threshold T_L and rejoining threshold T_H represent a more tolerant attitude to FDI attack, but it also increase the duration of the collective estimation error and the missed detection rate of the proposed control scheme.

5.5. Scalability Test of the Resilient Control Scheme

This study case investigates the scalability of the proposed resilient control scheme with a modified test microgrid system which is similar with the model in [9]. Figure 14 shows the electrical network and communication topology of the islanded microgrid system. The microgrid is composed of 10 DGs, and the related specifications of the model are listed in Table A1 in the Appendix A.

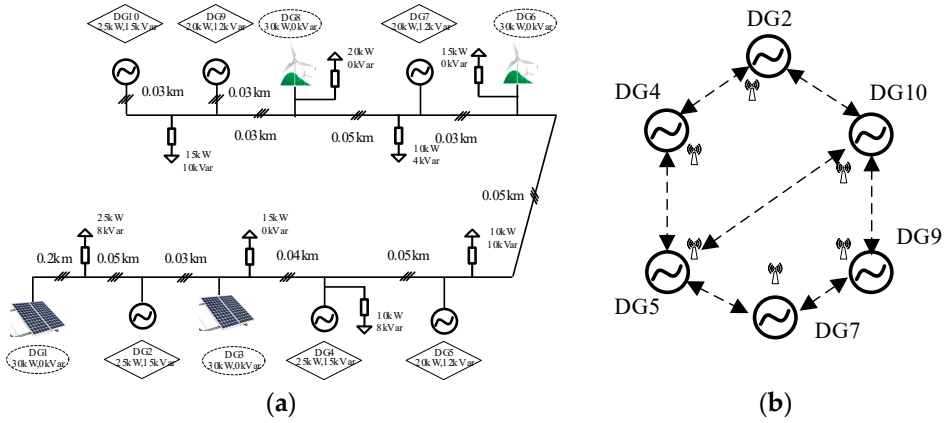

Figure 14. Modified microgrid test system: (**a**) Electrical network; (**b**) Communication topology.

As illustrated in Figure 14, DG1 and DG3 are photovoltaics (PVs), while DG6 and DG8 are wind turbines (WTs). PVs and WTs are not equipped with any storage device and operate in grid-feeding mode. This is standard practice and means that PVs and WTs are uncontrollable units, and they produce fixed amount of active power and no reactive power to the microgrid system, that is $Q_1 = Q_3 = Q_6 = Q_8 = 0$ [3,9]. Hence, the network possesses a total of six controllable DGs, e.g., micro gas turbine, and they are controlled by the proposed resilient control scheme. From t = 0 s, the microgrid works in islanded mode. At t = 1 s the secondary controller is applied and DG2 is under transient disturbance from 1.2s to 1.35s. The attack signals $f^a_{7,V}(k) = 0.7$ and $f^a_{7,Q}(k) = -150$ are

injected into DG7 from t = 2.5 s and removed at t = 3.5 s. The simulation results are demonstrated in Figure 15.

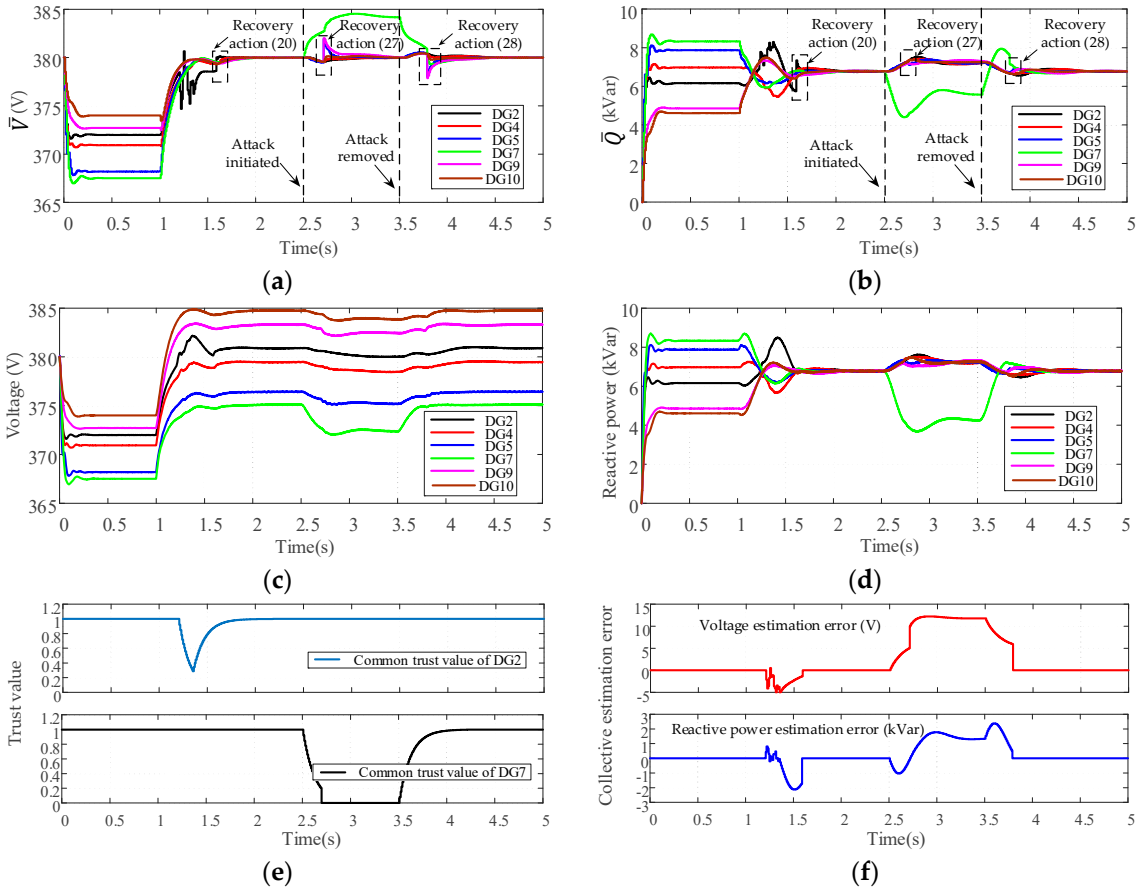

Figure 15. Performance of the control scheme under the scalability test: (**a**) Average voltage estimates; (**b**) Average reactive power estimates; (**c**) Voltages of DGs; (**d**) Reactive power of DGs. (**e**) Common trust values of DG2 and DG7; (**f**) Collective estimation error.

As can be seen in Figure 15, the proposed trust-based control scheme is able to eliminate the collective estimation errors caused by the transient disturbance or the FDI attack, which makes the average voltage and reactive power estimates converge to the correct consensus values. Thus, the objective of voltage restoration and reactive power sharing can still be achieved in both disturbance and attack scenarios, which verifies the scalability and resilience of the proposed control scheme.

6. Conclusions

In this work, a trust-based control scheme is developed in order to improve the resilience of the voltage and reactive power control of an islanded AC microgrid subject to FDI attack. The adverse impacts of FDI attack are described in detail according to the cumulative effects of injected signals, and the proposed resilient control scheme is tested in various attack scenarios.

The validation of the proposed method is carried out through simulations using MATLAB/Simulink toolbox. In both transient disturbance and continuous attack scenarios, the results have proved that the forward-backward criterion is able to detect the misbehaving DGs, and using the discarding information mechanism with the proposed recovery actions can prevent the propagation of false data as well as eliminate the collective estimation errors in the secondary controller of islanded microgrids. The proposed method is compared with the scheme only using the discarding information mechanism to prove that the recovery actions are necessary to maintain the correct average estimates of voltage and

reactive power. The capability to resist colluding attack and the scalability advantage of the proposed methods are also verified by case studies.

It can be obviously concluded that the proposed method can improve the resilience of the islanded microgrid, which ensures the average voltage restoration and reactive power sharing under FDI attack. In the future research, we will focus on the improvements of the trust-based control scheme while reducing the computation and communication burden.

Author Contributions: G.X. provided theoretical guidance. L.M. designed the trust-based resilient control scheme for the islanded microgrid and did the simulations to verify the effectiveness. All authors have read and agreed to the published version of the manuscript.

Funding: This work was supported by the Fundamental Research Funds for the Central Universities (2019QN111).

Conflicts of Interest: The authors declare no conflict of interest.

Appendix A

Table A1. Parameter values for simulation.

DG2, DG4, DG10	DG5, DG7, DG9
$R^f = 0.1\ \Omega \quad L^f = 1.35$ mH	$R^f = 0.1\ \Omega \quad L^f = 1.35$ mH
$R^c = 0.02\ \Omega \quad L^c = 2$ mH	$R^c = 0.04\ \Omega \quad L^c = 2$ mH
$m^P = 9.42 \times 10^{-5} \quad n^Q = 1.3 \times 10^{-3}$	$m^P = 12.56 \times 10^{-5} \quad n^Q = 1.5 \times 10^{-3}$
$K_{PV} = 0.1 \quad K_{IV} = 420$	$K_{PV} = 0.05 \quad K_{IV} = 390$
$K_{PC} = 15 \quad K_{IC} = 20,000$	$K_{PC} = 10.5 \quad K_{IC} = 16,000$
Line Impedance	
$0.642 + j0.083\ \Omega/\text{km}$	
Secondary Control Parameters	
$K_{PV}^{AVE} = 0.001$ $K_{IV}^{AVE} = 8$ $K_{PC}^{AVE} = 0.0001$ $K_{IC}^{AVE} = 0.025$ $\varepsilon = 0.06$	
Trust Evaluation Parameters	
$\alpha = 0.08$ $T_L = 0.2$ $T_H = 0.9$	

References

1. Kabalci, Y. A survey on smart metering and smart grid communication. *Renew. Sust. Energ. Rev.* **2016**, *57*, 302–318. [CrossRef]
2. Han, Y.; Zhang, K.; Li, H.; Coelho, E.A.A.; Guerrero, J.M. Mas-based distributed coordinated control and optimization in microgrid and microgrid clusters: A comprehensive overview. *IEEE Trans. Power Electron.* **2018**, *33*, 6488–6508. [CrossRef]
3. Schiffer, J.; Seel, T.; Raisch, J.; Sezi, T. Voltage stability and reactive power sharing in inverter-based microgrids with consensus-based distributed voltage control. *IEEE Trans. Control Syst. Technol.* **2016**, *24*, 96–109. [CrossRef]
4. Carpintero-Rentería, M.; Santos-Martín, D.; Guerrero, J.M. Microgrids literature review through a layers structure. *Energies* **2019**, *12*, 4381. [CrossRef]
5. Guerrero, J.M.; Vasquez, J.C.; Matas, J.; De Vicuna, L.G.; Castilla, M. Hierarchical control of droop-controlled AC and DC microgrids—A general approach toward standardization. *IEEE Trans. Ind. Electron.* **2010**, *58*, 158–172. [CrossRef]
6. Tran, Q.T.T.; Luisa Di Silvestre, M.; Riva Sanseverino, E.; Zizzo, G.; Pham, T.N. Driven primary regulation for minimum power losses operation in islanded microgrids. *Energies* **2018**, *11*, 2890. [CrossRef]
7. Isa, N.M.; Tan, C.W.; Yatim, A.H.M. A comprehensive review of cogeneration system in a microgrid: A perspective from architecture and operating system. *Renew. Sust. Energ. Rev.* **2018**, *81*, 2236–2263. [CrossRef]
8. Sonam, S.; Bidyadhar, S.; Susmita, D. Distributed voltage and frequency synchronisation control scheme for islanded inverter-based microgrid. *IET Smart Grid* **2018**, *1*, 48–56.
9. Chen, F.; Chen, M.; Li, Q.; Meng, K.; Guerrero, J.M.; Abbott, D. Multiagent-based reactive power sharing and control model for islanded microgrids. *IEEE Trans. Sustain. Energy* **2016**, *7*, 1232–1244. [CrossRef]

10. Simpson-Porco, J.W.; Shafiee, Q.; Dörfler, F.; Vasquez, J.C.; Guerrero, J.M.; Bullo, F. Secondary frequency and voltage control of islanded microgrids via distributed averaging. *IEEE Trans. Ind. Electron.* **2015**, *62*, 7025–7038. [CrossRef]
11. Abhinav, S.; Schizas, I.D.; Lewis, F.L.; Davoudi, A. Distributed noise-resilient networked synchrony of active distribution systems. *IEEE Trans. Smart Grid* **2018**, *9*, 836–884. [CrossRef]
12. Mahmoud, M.S.; Hamdan, M.M.; Barudi, U.A. Modeling and control of cyber-physical systems subject to cyber attacks: A survey of recent advances and challenges. *Neurocomputing* **2019**, *338*, 101–105. [CrossRef]
13. Chlela, M.; Joos, G.; Kassouf, M. Impact of cyber-attacks on islanded microgrid operation. In Proceedings of the Workshop on Communications, Computation and Control for Resilient Smart Energy Systems RSES '16, New York, NY, USA, 21–24 June 2016.
14. Deng, R.; Zhuang, P.; Liang, H. CCPA: Coordinated cyber-physical attacks and countermeasures in smart grid. *IEEE Trans. Smart Grid* **2017**, *8*, 2420–2430. [CrossRef]
15. Zhao, C.; He, J.; Cheng, P.; Chen, J. Analysis of consensus-based distributed economic dispatch under stealthy attacks. *IEEE Trans. Ind. Electron.* **2017**, *64*, 51107–55117. [CrossRef]
16. Rahman, M.A.; Mohsenian-Rad, H. False data injection attacks with incomplete information against smart power grids. In Proceedings of the 2012 IEEE Global Communications Conference (GLOBECOM), Anaheim, CA, USA, 3–7 December 2012.
17. Liang, G.; Zhao, J.; Luo, F.; Weller, S.R.; Dong, Z.Y. A review of false data injection attacks against modern power systems. *IEEE Trans. Smart Grid* **2017**, *8*, 1630–1638. [CrossRef]
18. Qi, J.; Taha, A.F.; Wang, J. Comparing kalman filters and observers for power system dynamic state estimation with model uncertainty and malicious cyber attacks. *IEEE Access* **2018**, *6*, 77155–77168. [CrossRef]
19. Zhao, J.; Zhang, G.; La Scala, M.; Dong, Z.Y.; Chen, C.; Wang, J. Short-term state forecasting-aided method for detection of smart grid general false data injection attacks. *IEEE Trans. Smart Grid* **2017**, *8*, 1580–1590. [CrossRef]
20. Wang, H.; Ruan, J.; Ma, Z.; Zhou, B.; Fu, X. Deep learning aided interval state prediction for improving cyber security in energy internet. *Energy* **2019**, *174*, 1292–1304. [CrossRef]
21. James Ranjith, K.R.; Kundur, D.; Sikdar, B. Transient model-based detection scheme for false data injection attacks in microgrids. In Proceedings of the 2019 IEEE International Conference on Communications, Control, and Computing Technologies for Smart Grids (SmartGridComm), Beijing, China, 21–23 October 2019.
22. Zhang, H.; Meng, W.; Qi, J.; Wang, X.; Zheng, W.X. Distributed load sharing under false data injection attack in an inverter-based microgrid. *IEEE Trans. Ind. Electron.* **2019**, *66*, 1543–1551. [CrossRef]
23. Beg, O.A.; Johnson, T.T.; Davoudi, A. Detection of false-data injection attacks in cyber-physical DC microgrids. *IEEE Trans. Ind. Electron.* **2017**, *13*, 2693–2703. [CrossRef]
24. Beg, O.A.; Nguyen, L.V.; Johnson, T.T.; Davoudi, A. Signal temporal logic-based attack detection in DC microgrids. *IEEE Trans. Smart Grid* **2019**, *10*, 3585–3595. [CrossRef]
25. Abhinav, S.; Modares, H.; Lewis, F.L.; Ferrese, F.; Davoudi, A. Synchrony in networked microgrids under attacks. *IEEE Trans. Smart Grid* **2018**, *9*, 6731–6741. [CrossRef]
26. Chen, L.; Wang, Y.; Lu, X.; Zheng, T.; Wang, J.; Mei, S. Resilient active power sharing in autonomous microgrids using pinning-consensus-based distributed control. *IEEE Trans. Smart Grid* **2019**, *10*, 6802–6811. [CrossRef]
27. Zeng, W.; Chow, M. Resilient distributed control in the presence of misbehaving agents in networked control systems. *IEEE Trans. Cybern.* **2014**, *44*, 2038–2049. [CrossRef] [PubMed]
28. Ren, J.; Zhang, Y.; Ye, Q.; Yang, K.; Zhang, K.; Shen, X.S. Exploiting secure and energy efficient collaborative spectrum sensing for cognitive radio sensor networks. *IEEE Trans. Wirel. Commun.* **2016**, *15*, 6813–6827. [CrossRef]
29. Singh, K.; Verma, A.K. FCTM: A novel fuzzy classification trust model for enhancing reliability in flying Ad hoc networks (FANETs). *Ad Hoc Sens. Wirl. Netw.* **2018**, *40*, 23–47.
30. Zhu, M.; Martínez, S. Discrete-time dynamic average consensus. *Automatica* **2010**, *46*, 322–329. [CrossRef]
31. Shafiee, Q.; Guerrero, J.M.; Vasquez, J.C. Distributed secondary control for islanded microgrids—A novel approach. *IEEE Trans. Power Electron.* **2014**, *29*, 1018–1031. [CrossRef]
32. He, J.; Zhou, M.; Cheng, P.; Shi, L.; Chen, J. Consensus under bounded noise in discrete network systems: An algorithm with fast convergence and high accuracy. *IEEE Trans. Cybern.* **2016**, *46*, 2874–2884. [CrossRef]

33. Zeng, W.; Chow, M. A reputation-based secure distributed control methodology in D-NCS. *IEEE Trans. Ind. Electron.* **2014**, *61*, 6294–6303. [CrossRef]
34. Li, P.; Liu, Y.; Xin, H.; Jiang, X. A robust distributed economic dispatch strategy of virtual power plant under cyber-attacks. *IEEE Trans. Ind. Inform.* **2018**, *14*, 4343–4352. [CrossRef]
35. Jones, G.; Vanderson, B.; Otto, L.; Edson, S.; Jean-Paul, B.; Fabrício, E. Trust and reputation models for multi-agent systems. *ACM Comput. Surv.* **2015**, *48*, 1–42.
36. Hao, Y.; Cheng, Y.; Zhou, C.; Song, W. A distributed key management framework with cooperative message authentication in VANET. *IEEE J. Sel. Areas Commun.* **2011**, *29*, 616–629. [CrossRef]
37. Zhang, Q.; Yu, T.; Ning, P. A framework for identifying compromised nodes in wireless sensor networks. *ACM Trans. Inf. Syst. Secur.* **2008**, *11*, 1–37. [CrossRef]